Development of a High-Performance Compact Refrigeration Cooling Prototype

By

Mahmoud Abdel Rahman Alzoubi

A Thesis Presented to the

Masdar Institute of Science and Technology

in Partial Fulfillment of the Requirements for the Degree of

Master of Science

In

Mechanical Engineering

Abstract

Reliability and performance of high power-density devices can be enhanced through deployment of efficient cooling systems. Compact refrigeration cooling systems offer distinct benefits for use in portable and small-scale applications compared to other technologies. They can work at high ambient conditions and provide uniform device cooling. In order to reduce the redundancy of conventional refrigeration systems, this thesis aims at developing a compact recuperator-based Vapor Compression Cycle (VCC) prototype. The VCC system composes of a 300W linear compressor and fluid-to-fluid recuperator that utilize the temperature difference between condenser and evaporator. Comprehensive guidelines to design and build a test-bed setup are presented with all related aspects such as material selection, test-bed construction, leakage test procedure, insulation, and refrigerant charges. Several parametric studies are performed to investigate the influence of changing the compressor capacity, heat source temperature and expansion valve opening position on the VCC performance. Component models for linear compressor, fin-tube heat exchanger, brazed plate heat exchanger, and metering valve are developed and validated with the experimental data. These component models are further integrated to predict the pressure and temperature changes in the VCC test-bed. In the compressor model, increasing piston velocity and piston stroke distance lifts the exit pressure and temperature. Heat exchanger characteristics indicate that the pressure drop is negligible due to low refrigerant flow rate. There are several advantages to use the recuperator-based VCC configuration. The refrigerant exiting the condenser heats the refrigerant flow at the evaporator exit to maintain the superheated flow at the compressor inlet. With this design, the condenser size could be reduced, which leads to a more compact system. Meanwhile, the evaporator is able to extract more heat from the heat source by maintaining two-phase refrigerant flow between the inlet and exit. As a result, the cooling test-bed was able to achieve a high coefficient of performance (COP) of 4.5. This study contributes to the development of energy-efficient compact VCC systems for various cooling applications.

This research was supported by the Government of Abu Dhabi to help fulfill the vision of the late President Sheikh Zayed Bin Sultan Al Nahyan for sustainable development and empowerment of the UAE and humankind.

Acknowledgments

I am firstly grateful to Almighty Allah for giving me the strength and ability to develop and complete this master's thesis. Secondly, I would like to thank Dr. TieJun (TJ) Zhang, my advisor, for his endless support, encouragement and trust throughout my study at Masdar Institute. He employed most of his effort, time, and knowledge to improve my performance and reinforce my scientific fundamentals understanding. Also, I would like to thank my Research Supervisory Committee members: Dr. Tariq Shamim and Dr. Peter Armstrong for their support and advise to enrich this research. I would especially thank Dr. Peter Armstrong for his efforts and detailed comments on my thesis.

I wish to thank Masdar Institute of Science and Technology for the scholarship and the financial support of this study. I also wish to appreciate all of my colleagues at Renewable Thermal Energy (RTR) Lab for their tremendous support. Special thanks to Dr. Guanqui Li for his friendship, his ethics and moral support. Dr. Li assisted me in selecting the prototype's components and building the experimental setup. To Charles C. Okaeme and Alexander R. Higgo, I am grateful to have two more brothers. You have my gratitude for your understanding, support and more importantly your friendship. A special acknowledgment of the calibration of the air velocity instrument calibration by Alex Niswander and Munira Sibai

Lastly I would like to thank my family for their endless care, support and believing in my competence to finish this step in my life. To Ruba N. Yousef, my wife, without you, this journey could not be done. I love you.

Mahmoud A. Alzoubi

Masdar City, June 29, 2014.

Contents

List of Tables

List of Figures

Chapter 1

Introduction

1.1 Vapor Compression Cycle

Air conditioning systems are used extensively in several applications such as domestic, commercial, electronics, and transportation cooling applications. All these cooling applications are very energy intensive and consume up to 70% of the UAE total energy consumption [1]. Hence, better designs of cooling systems are required to minimize this percentage. The trend in electronic industry is towered more compact systems. These systems required more effective cooling as they produce a lot of heat. Hence, Compact vapor compression cycles (VCC) are sought after which have higher performance, required less material, smaller footprint and they can be used as portable systems.

To achieve the maximum cooling performance required by the compact applications, the flow at evaporator should remain in two phase region. Two phase flow is preferable because it takes the advantage of latent heat that associated with the phase change which contributes to a higher heat transfer coefficient. With higher heat transfer coefficient uniform cooling with better heat removal is achievable. This work focuses on developing a recuperator-based high-performance compact VCC prototype. Comprehensive guidelines to design, build, test, model and operate a VCC test-bed is proposed.

In 1755, Professor William Cullen (Scotland), designed the first artificial refrigeration system. A container with diethyl ether was exposed to a partial vacuum, using a small pump. The diethyl ether then boiled and absorbed heat from the surrounding air. This experiment even created a

small amount of ice [9]. Although the experiment had no practical application at that time, it inspired scientists and inventors around the world to develop a wide variety of refrigeration systems in the last century. Today, vapor compression cycles(VCC) are widely used in refrigeration and air conditioning systems that are considered as one of the most important energy-consuming domestic appliances. Refrigerators and air conditioning systems represent 13.7% and 16% respectively of all residential electricity consumption in USA for 2001 [12]. Hence, much research has been done to study and analyze the cooling performance for these cycles. Chen et al. [18] derived the relations between the COP (coefficient of performance) and pressure ratio for an air refrigeration cycle. They conducted their experiment with a constant and a variable temperature heat sink. They found that COP and cooling load are strongly related to the thermal conductance rate of the heat reservoirs, the effectiveness of the condenser and evaporator and the component efficiencies. Nnanna [46] studied the transient response of the VCC to rapid change in evaporator heat load. He fabricated his experiment specially for applications to cool high heat flux electronics. His VCC prototype revealed fluctuations in temperature during the early stage of the cooling process. Also, the response time for the change in evaporator loads was varied. Arora and Kaushik [8] presented detailed analysis of a VCC test-bed. In there research, they developed a model to compute the cycle COP and exergetic efficiency for different refrigerant. They performed their experiment with evaporator and condenser temperature range from -50 ^{o}C to 0 ^{o}C and 40 ^{o}C to 55 ^{o}C respectively. They found that when the evaporator temperature increases, the pressure ratio across the compressor decreases which lead to a lower compression work and then a higher COP. They also concluded that sub-cooling the condensed refrigerant can improve the COP of the cycle. Additionally, they found that any increase in the pressure drop across the evaporator or condenser will reduce the COP.

In order to enhance the COP of the refrigeration systems, many investigators have been conducted on VCCs and new cycle configurations. Torrella et al. [55] described a general methodology for analyzing six possible configuration of VCC. They found that configuration with higher subcooling degree has higher COP, due to the fact that the degree of subcooling increases the difference in specific enthalpy across the evaporator. Jensen and Skogestad [29] focused on the optimal operation for a simple VCC. They discussed the effect of having sub-cooling and superheating on the compressor power consumption. They found that super-heating degree should be minimized whereas some sub-cooling is optimal.They also, found that for a simple ammonia

VCC, sub-cooling before the expansion valve by 4.66 ^{o}C save about 1.74% of the compressor power consumption. Klein et al. [34] studied the effect of using a liquid-suction heat exchanger on the VCC performance. They discussed the relation between the heat exchanger effectiveness and the cycle COP. They found that using liquid-suction heat exchanger will increase refrigerant temperature and decrease its pressure before entering the compressor which decreases the compressor volumetric efficiency. They mentioned that the disadvantages of using these heat excahnger are the slightly increase in the compressor power consumption and the pressure drop in the heat exchanger. Mastrullo et al. [40] studied the influence of using recuperator heat exchanger on the refrigeration system. They used 19 different refrigerant and performed their experiment with evaporator and condenser temperature range from -40 ^{o}C to 10 ^{o}C and 25 ^{o}C to 50 ^{o}C respectively. They concluded that benefit of using the recuperator on the system COP depends on the fluid thermo-physical properties and system operation conditions. They found that the presence of heat exchanger has higher positive influence if a fluid with low COP is used, and low positive influence is a refrigerant with high COP is used in the VCC. However, the presence of the recuperator has the same effect on the COP and the volumetric efficiency. Aprea et al. [7] discussed the advantages of using suction-liquid heat exchanger on the performance of refrigeration systems from a thermodynamic point of view. They discussed the influance of using the recuperator in enhancing the COP by adding some sub-cooled and super-heated degrees on the refrigerant. They evaluated the ratio of heat gain in the recuperator-based system into the normal specific latent heat at different evaporation temperature and different refrigerants. The ratio increased with increasing the evaporation temperature.

Compact refrigeration cooling systems offer distinct benefits for use in portable and small-scale applications such as electronic cooling. They provides uniform cooling temperature, due to the two-phase heat transfer in the evaporator. Wu and Du [58] presented a VCC for electronics cooling with cooling capacity of 200W. They used a cold plate with cartridge heater and heat spreader for the evaporator side to simulate the heat generated from the electronic chips. Throughout their experiments, they found that the capillary tube length and the amount of refrigerant charge are important to deliver the desired evaporating temperature. Also, they calculated the system second-law efficiency which was varied from 23% to 31%. Trutassanawin et al. [56] developed a compact refrigeration system prototype to demonstrate its feasibility for use in electronic cooling. The system cooling capacity varied from 121 to 268 W, with a COP of

2.8 to 4.7, and with a second-law efficiency ranging from 33% and 52%. The system was able to keep the temperature of a chip size 1.9 cm^2 at 85 ^{o}C. Mancin et al. [39] built a water cooled miniature scale refrigeration system test bed that implements a linear compressor prototype and a cold plate at the evaporator side. Based on the operating test conditions, they found that, at any evaporation temperature, the heat dissipated by the cold plate increased as the piston stroke increased. Furthermore, at constant compressor stroke, the cooling capacity increased when decreasing and increasing the condenser and evaporator temperatures respectively. Chang et al. [16] examined the thermal performance of a miniature VCC for electronic cooling purposes. They studied the effect of the compressor speed and the expansion valve opening on the COP of the cycle. Also, they explained the effect of the compressor speed and the expansion valve opening on the condensation phenomena at the the inlet and outlet of the evaporator. They found that the condensation phenomena were improved when the compressor speed was reduced from 4200 to 3840 RPM.

1.2 Linear Compressor Modeling

Compressors are the main moving components in the refrigeration cooling systems. They increase the refrigerant pressure, reduce its volume and transport it through VCC pipes. Despite the similarity of the compressors work, Linear compressor has the inherent advantage for refrigeration applications since it can be easily controlled to provide variable refrigeration cooling capacities upon demand. High-performance compact compressors are desired, particularly in small-scale applications. Comparing with other types of compressors, linear compressors have fewer moving parts and smaller footprint. These advantages are attracting more advanced research on linear compressors. Many studies have been done on the common compressor types, including scroll and screw compressors. New-type compressors such as linear compressors still require more research effort. Bradshaw et al. [14] provided a detailed model to define the working principle of a linear compressor. Their model incorporated all of the major components of the linear compressor. They discussed the force balance across the reed valves. They also modeled the refrigerant leakage inside compressor and considered the leakage between the piston and the compression chamber wall as the dominant leakage. Additionally, their model incorporated the dynamics associated with the piston motion, they discussed the effect of the motor vibration on the useful driving force of the piston. Ribeiro [51] developed and analyzed a com-

pact VCC using a linear compressor. He used a linear compressor manufactured by Embraco company. He ran the experiment at different ambient temperatures and different compressor speeds. He found that the cooling capacity and COP increased with decreasing the ambient temperature. Also, the cycle achieved higher cooling capacities when the compressor worked at its full piston displacement. Rigola et al. [52] developed a numerical simulation model for thermal and fluid dynamic optimization of a reciprocating compressor. They validated their model with experimental data. Their model focused on the effect of the compressor geometry, the motor specifications and the working conditions on the volumetric and isentropic efficiency of the compressor in addition to the COP. They found that the diameters of the suction and discharge valves affect the volumetric efficiency and the COP. They observed that there are optimal values for the discharge valve diameter and the suction valve stop to give a good volumetric efficiency and adequate COP. On the other hand, they found that the suction valve diameter and discharge valve stop values should be large enough, but within a range, to increase the volumetric efficiency and COP. However, if these values exceed their range, higher values will reduce the optimal values of the volumetric efficiency and COP. At the end, they highlighted the effect of changing the evaporation temperature and the compressor speed on the COP. They found that increasing the evaporating temperature and the compressor speed will enhance the COP. Kim and Jeong [33] discussed the performance, the capacity modulation and variable stroke mechanism of a controlled linear compressors vs a non-controlled compressor. They mentioned that linear compressor can modulate its capacity independently without any stroke control. They found that the controlled compressor has lower power consumption than the uncontrolled compressor. Liang et al. [38] designed a linear compressor for electronics cooling applications. They found that the lowest power consumption and the highest COP and efficiency is at the drive resonance frequency. The compressor showed a reduction in the COP by 12% and required 11% extra electrical power input. Also, they showed in their calculation how COP increased with increasing the cooling capacity as the evaporator temperature raised. Kim et al. [30] presented experimental and numerical results of dynamic characteristic and COP of a linear compressor. They discussed also, the effect of system resonance on the compressor performance. They concluded the same as Liang et al. [38] that power consumption and volumetric losses due to low stroke displacement can be minimized at the system resonance. Perez-Segarra et al. [48] conducted a detailed analysis of the volumetric and isentropic efficiencies. They presented these efficiencies in their main components. They showed that both efficiencies reduced when the pressure ratio

across the compressor increased. Also, they mentioned that the volumetric efficiency increased with increasing the evaporation temperature.

1.3 Hydrocarbons as Refrigerants

Over the past decades, traditional refrigerant such as chlorofluorocarbon (CFC), hydrochlorofluorocarbon (HCFC), and hydrofluorocarbons (HFC) have been used extensively in refrigerators and air conditioning systems because of their excellent chemical and thermophysical properties. However, the growing concerns about climate change, global warming and other environmental problems led to replace the CFCs and HCFCs by HFCs gases because of their high ozone-depletion potential (ODP)and global warming potential (GWP). HFCs have zero ODP but their GWP is relatively high. Therefore, many investigations have been conducted to find environmentally friendly gases to replace the currently used refrigerants. Among different choices, hydrocarbon gases (HCs) that have zero ODP and negligible GWP are considered as a strong alternative to replace HFCs. Mohanarj et al. [42] reviewed several experimental and theoretical studies that have been carried out with HCs and HCs/HFCs mixtures. In their review, they discussed the environmental impacts (ODP and GWP) from using the traditional CFCs, HCFCs and HFCs gases. They also reviewed several experimental studies that compared the performance of HCs and traditional refrigerant in air conditioning and heat pumps applications. They concluded from their review that cooling systems with HCs and HCs/HFCs mixtures provided better performance than the currently used refrigerant. Additionally, HCs are found to be the best long-term alternatives to CFCs, HCFCs and HFCs refrigerants. Palm [47] reviewd the properties and performance of different HCs as refrigerants in small refrigeration systems and compared the result with R22 and R134a. He also studied the compatibility of HCs with the construction materials as metal alloys and polymers that used with the current refrigerants. He concluded that COPs of HCs were equal or higher than those of R22 and R134a. Also, it was shown that HCs were compatible with the systems components that used with R22 and R134a. Ayub [10] discussed the compatibility of hydrocarbons and other natural gases with currently used heat exchangers. He mentioned that ammonia (R717) is not compatible with copper and copper alloys. On the other hand, hydrocarbons gases have the advantage of being compatible with almost all currently used heat exchangers.

Several studies and experiments have been conducted to study the HCs chemical and thermo-physical properties, assess their COP, cooling capacity and power consumption in cooling and heat pumps systems and compare them with the currently used refrigerants. Lee et al. [37] conducted an experiment to compare the condensing heat transfer coefficient and the pressure drop for HCs and one of the common CFC gases (R22). They used a horizontal double pipe heat exchanger for their experiment. They found that the condensing heat transfer coefficient of HC refrigerants were higher by at least 31% than R22. However, they concluded from their experiment that HC refrigerant had higher pressure drops than R-22 by at least 50%. Navarro et al. [45] conducted comparative studies between R1234yf, R134a and propane (R290) at two different compressor speeds and evaporating temperature from -15 ^{o}C to 15 ^{o}C. They found that propane had a significantly higher volumetric and compressor efficiencies by about 30% and 15% respectively, and lower heat losses than the other two refrigerant which can reduce the refrigerant charges for same system size. Also, they found that R134a had the highest heat losses among the three selected refrigerant. Cheng et al. [20] performed experiments to compare the performance of R32, R290, R410A and R22 refrigerants. The charge for R290 was about 50% less than R22. Nevertheless, they found that the power consumption of R290 was about 18% lower than R22, the COP of R290 was 20.4% higher than R22, and the discharge temperature of R290 was ranging from 60 ^{o}C to 70 ^{o}C while the R22 discharge temperature was around 90 ^{o}C. Wu et al. [57] studied the performance of a small through-wall room air conditioner by using R290 and R22. They compared the COP, efficiency efficiency ratio (EER) and power consumption for both gases. The experiments were carried out under same conditions. They showed that the COP of R290 was about only 5% lower than R22 but with a charge 50% less than R22. Also, the power consumption of R290 was 13.9% lower and the EER was 10.3% higher than R22 with the same charges difference. Al-Rashed [5] evaluated different refrigerants in his research. He compared the COP of R290 and isobutane (R600a) with R22, R134a and R410A refrigerants. He conducted his experiments at different condensing temperatures (38 ^{o}C and 45 ^{o}C) and different finned-tube evaporator arrangements. In all cases, he found that HCs performed better at lower condensing temperature, and generally they had better or equal COP than R22 and R134a. Chang et al. [17] investigated the performance of a heat pump system using different HCs gases (R290, R600a, butane (R600), and propylene (R1270)) and compared them with the performance of R22. They found that the cooling and heating capacity of R290 are slightly lower than those of R22 but their COP are slightly higher at the same compressor speed.

Ahamed et al. [3] studied the exergy losses, exergy efficiency, second law efficiency and irreversibility of a VCC that used R600a, R290 and R134a as working fluids. They conducted their experiments at different evaporating and condensing temperatures. They found that the lowest losses occurs in the expansion device while the compressor has the highest exergy losses. They also, compared the exergy efficiencies for the different gases and found that HCs have about 50% higher exergy efficiency than R134a. Additionally, both R290 and R600a showed higher COP than R134a at different evaporating temperature. Lampugnani and Zgliczynski [36] analyzed the impact of using R290 in VCCs running with hermetic compressors. They compared the performance of R290 with R22 in terms of COP, cooling capacity, volumetric capacity, and pressure ratio. They concluded that R290 has strong potential to replace R22 in domestic and commercial air conditioning systems. They built their conclusion based on the performance of R290. They found that the COP of R290 was about 5% higher than R22. Also, the pressure ratio and volumetric capacity were 12-18% and 13-14% lower than R22 respectively. Hammad and Alsaad [28] evaluated the performance of different HCs and HCs mixture versus traditional R-12 refrigerant. Their research showed that the COP of pure R290 was higher than any other HCs mixtures and also higher than R-12 at different evaporating temperatures. Also, the compressor power consumption of R290 was around 17% lower than R-12.

Hydrocarbons as refrigerants are considered as a strong alternative for CFCs, HCFCs, and HFC. They have better performance, better power consumption, minimal changes in the systems' components, and the most important they need smaller charges to reach the same cooling capacity and COP of the traditional refrigerants. However, the main concerns about using HCs are fire and explosion hazards due to the flammability of these gases. Many studies have been conducted discussing these concerns and mentioning the standards, regulations, and procedures for using HCs safely in cooling systems. Colbourne and Sueh [23, 24] described a quantitative risk assessment (QRA) model to assess the hazardous potential of using HCs as refrigerant in cooling systems. Their model described in details the criteria of considering the usage of HCs has a potential for ignition. The model discussed the refrigerant leakage, the flammable volume and flammable time, and source of ignition. They concluded that the ignition potential is not an absolute value related only to the HCs usage. Granryd [27] discussed the opportunities and concerns of using hydrocarbons as cooling fluid. He reviewed different hydrocarbon gases thermophysical properties. He concluded that hydrocarbons are interesting refrigerant alternatives

for energy efficient and environmentally friendly refrigeration systems. However, he mentioned that safety precautions must be taken due to gases flammability. Compact refrigeration cooling systems have the advantage of minimizing refrigerant charges. Corberan et al.[25] reviewed the standards and regulations of using hydrocarbons as refrigerant. They reviewed the refrigerant charge limits as per the international standards. They also, discussed the ventilation requirements for the room where the cooling systems is installed and the ventilation of the enclosure if the systems installed within cabinets. They also, mentioned the requirements for safe design and construction cooling systems. Finally, they mentioned that the only argument against using hydrocarbons is the safety concern in handling large charges of hydrocarbons and having the expertise to install and maintain the system. Therefore, the key success of applying hydrocarbons to any refrigeration system is relying on the charge minimization by using miniature cooling system.

1.4 Objectives and Overview

The objective of this work is to design and build a recuperator-based compact VCC with linear compressor that use R134a as its working fluid. In addition, component level and cycle level modeling are to be performed. To accomplish this objective a combination of modeling and extensive experimental efforts are used.

Chapter 2 shows further details about designing and building VCC. Component assembly, leakage test procedure, refrigerant charging and other strict procedures that should be followed in order to construct a VCC test-bed are described extensively.

Chapter 3 talks about VCC operation guidance. It mentions the important steps of starting-up and shutting down the system. The parametric studies that will be handled in this work, such as changing compressor capacity, heat source temperature and expansion valve opening position, are also discussed in detail. Chapter 3 also discusses and analyzes the steady state dynamics of the system at different operation points. It illustrates the effect of changing system variables on the overall cycle behavior and performance.

Chapter 4 discusses VCC component and cycle-level model and validation. Fin-tube condenser

and plate heat exchanger evaporator models are developed to predict heat transfer in these heat exchangers. Component models are combined and integrated into a cycle model. Models validation with the experimental results is also handled.

Chapter 2

VCC Experimental Test-bed

2.1 Test Bed Design

There are different designs to build a VCC. Torrella et al. [55] described six configurations and compered the COPs for each one. The basic design is to have a compressor and an expansion device connected to each other through an evaporator and a condenser as shown in Figure 2.1.

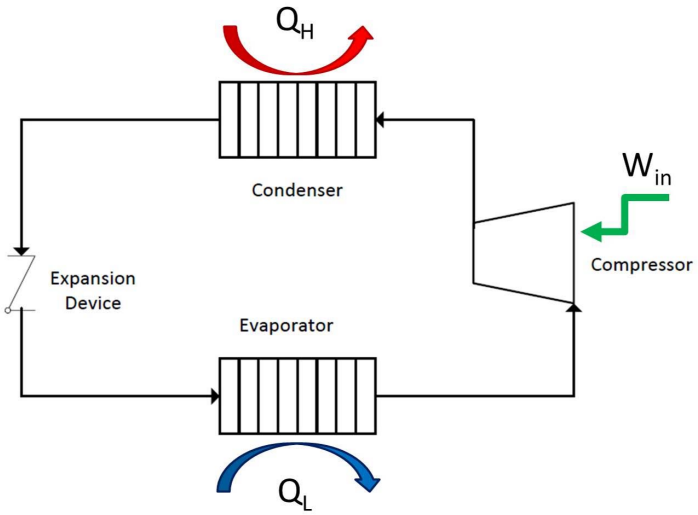

Figure 2.1: Schematic diagram of a basic vapor compression cycle

The COP of a cooling system is the ratio of the evaporator cooling effect to the compressor and condenser fan power consumption. One way to enhance the performance of a cooling system is by increasing its cooling capacity:

$$COP = \frac{Desired\ Output}{Required\ Input} \tag{2.1}$$

Figure 2.2 shows P-h diagram of a basic VCC. The cooling capacity and the enthalpy difference are related as below:

$$\dot{Q} = \dot{m}\Delta h \tag{2.2}$$

The enthalpy difference between the expansion device and the compressor can be increased by adding sub-cooling degrees before the expansion device and super-heating degrees after the evaporator.

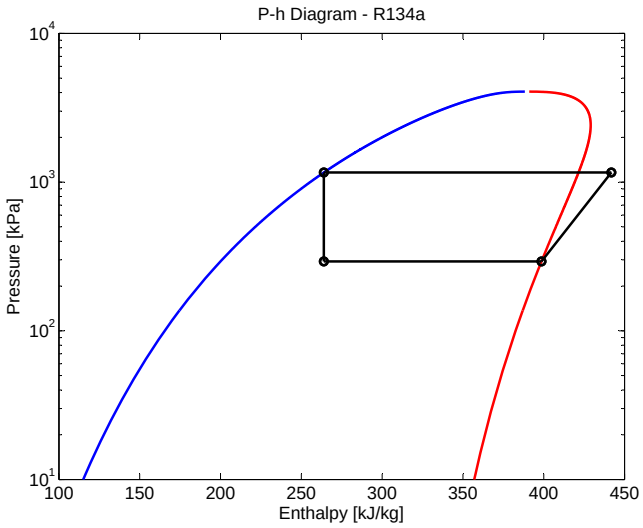

Figure 2.2: P-h diagram of an ideal vapor compression cycle

For better heat transfer in the evaporator and to prevent the critical heat flux (CHF) [41], an accumulator is usually added after the evaporator so, the evaporator exit will be maintained in the two-phase flow region [15]. On another hand, an internal heat exchanger can be added to utilize the temperature difference in the loop by exchanging the heat between the condenser exit and evaporator exit as described in Figure 2.3. This will add some sub-cooling degrees before the expansion device and super-heating degrees before the compressor inlet.

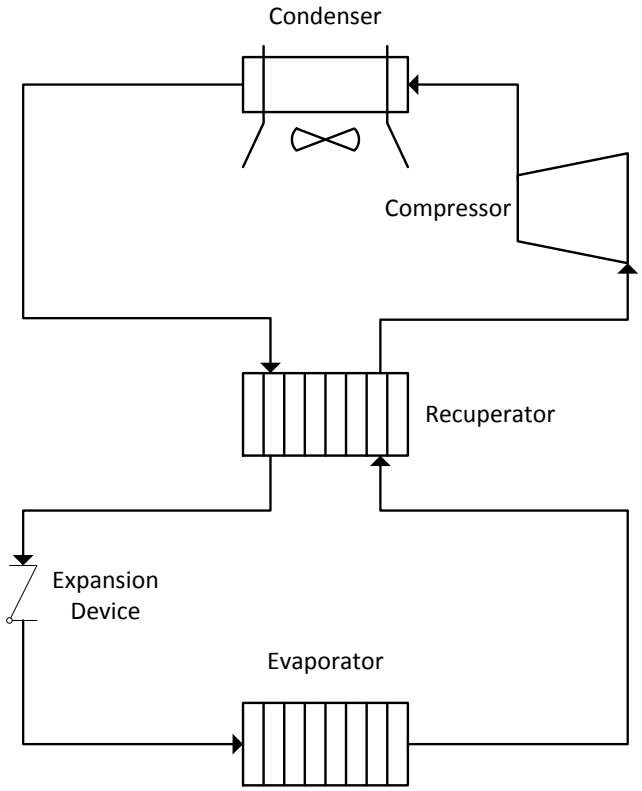

Figure 2.3: Schematic diagram of a vapor compression cycle with recuperator

The VCC schematic in Figure 2.3 is the design base of the test-bed in this work. The loop consists of main components in addition to auxiliaries that needed to run the experiments smoothly and to be able to measure and collect the required data. A detailed schematic diagram of the test-bed is shown in Figure 2.4. The schematic shows the place of the auxiliaries such as the flow meters, filter drier, and others. Also, it shows the place of each measuring components, the connection size, and the place of the charging and discharging ports. Additionally, it shows the details of the secondary loop between the evaporator and the temperature control bath (TCB) (the heat sink).

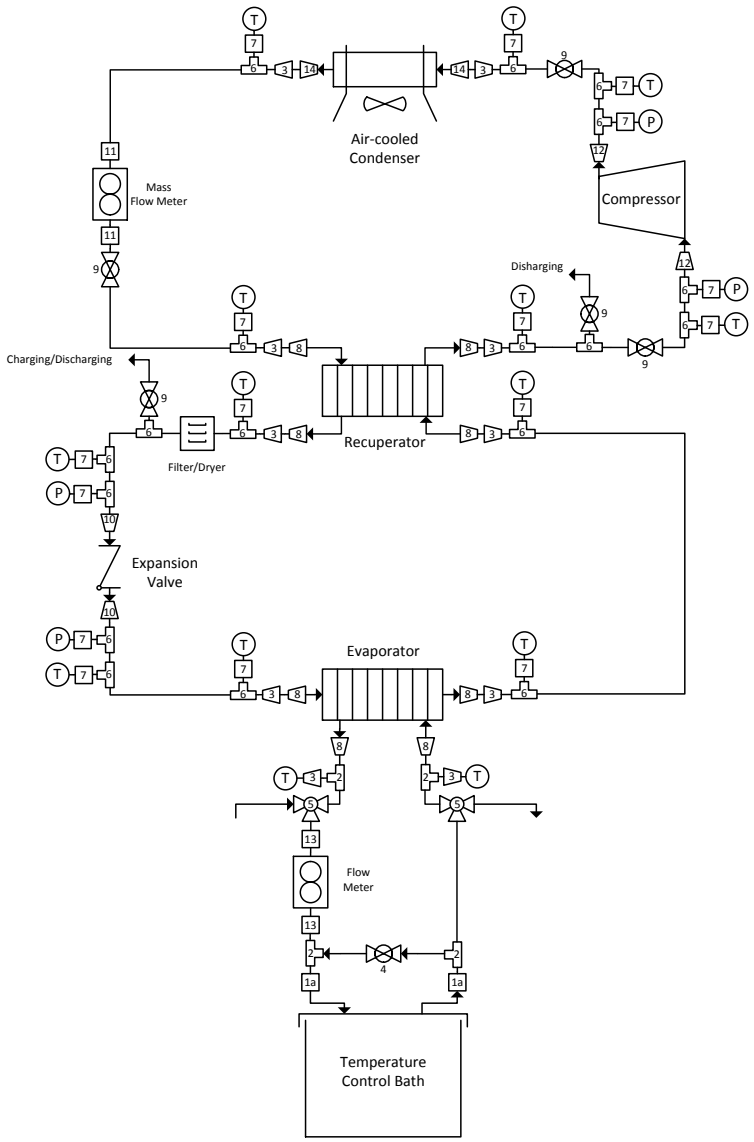

Figure 2.4: Detailed design of VCC test-bed setup

The test-bed uses 15 thermocouples to read the temperatures at the inlet and exit of each component in addition to the ambient temperature. Also, four absolute pressure transducers are placed at the inlet and exit of the compressor and the expansion device. Two mass flow meters measure the refrigerant flow rate in the main loop and the oil flow rate from the TCB in the secondary loop.

2.2 Material Selection

2.2.1 Main Components

1. **Compressor**

   An oil free, single acting linear compressor from Embraco Company is used in this work as shown in Figure 2.5.

Figure 2.5: 300W Linear Compressor

The compressor is controlled by an electronic control unit as depicted in Figure 2.6. This unit powers the compressor by converting a 24VAC-50Hz input voltage into a variable output voltage up to 12VAC. Also, it can power a small fan to cool the compressor shell if required. The compressor is controlled throughout a decent software as shown in Figure 2.7.

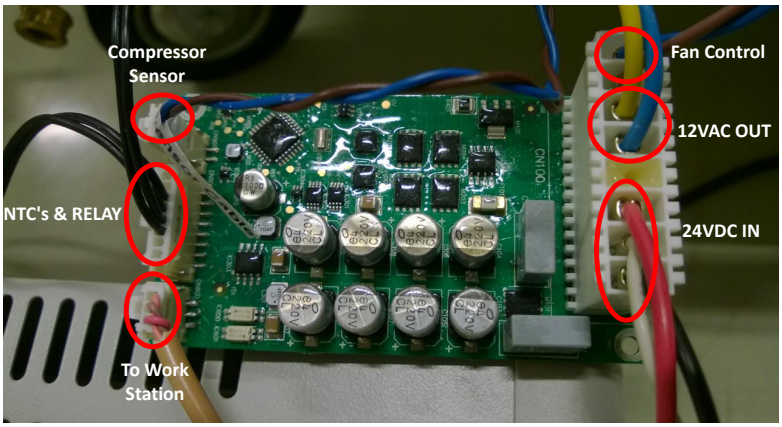

Figure 2.6: Electronic Control Unit

The program provides two different operation modes - continuous and timed. In the timed

mode, the user sets the period that the compressor should stay on. Also, the program allows the user to control the on-off temperature.

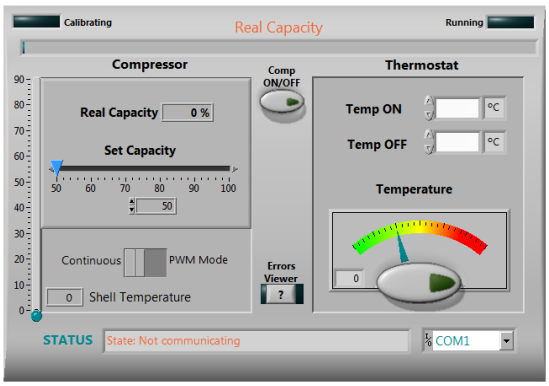

Figure 2.7: Compressor control program

If the room temperature reaches a certain value the compressor will run until reaching the off-temperature. Additionally, the program has an indicator for the compressor shell temperature and provides error indicators if the compressor stops working as shown in Figure 2.8.

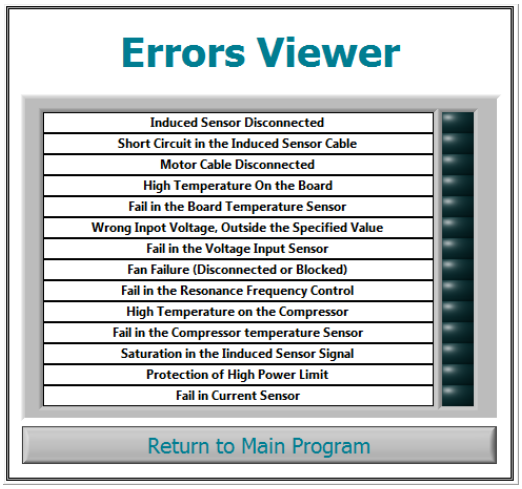

Figure 2.8: Errors viewer

The advantages of using linear compressor are discussed in detail elsewhere [13, 51, 48, 30]. In addition to its oil-free operation, linear compressor has fewer moving parts and the smallest footprint compared to other types. These inherent advantages make linear compressor the first choice to build a compact VCC test-bed. The nominal capacity of the compressor is 300 W with a 20 bar maximum pressure difference. Table 2.1 lists the

main specifications of the compressor.

Description	Data
General Information	
Suction [mm]	4.76
Discharge [mm]	4.76
Mechanical Data	
Displacement [cm^3]	0.267
Weight [kg]	1.30
Application	
Maximum Ambient Temperature [°C]	60
Maximum Shell Temperature [°C]	80
Maximum Condensing Pressure [kPa]	2,942
Pressure Difference Maximum (ΔP)[kPa]	1,961.3
Electrical Data	
Nominal Inverter's Input Voltage [Vdc]	24
Motor Type	Linear
LRA - Locked Rotor Amperage [A]	11
FLA - Full Load Amperage [A]	11

Table 2.1: Linear Compressor Specification

2. **Air Cooled Condenser**

   A fin-tube, fan cooled heat exchanger is used to cool the refrigerant and reject its excess heat to the environment as shown in Figure 2.9.

Figure 2.9: Fan-cooled condenser

The condenser is provided with a built-in single speed fan. The condenser consists of 20 tubes-bank connected to each other by return bends as depicted in Figure 2.10. The inlet diameter of the pipe is 7 mm and the total length of the tubes-bank is 5.4 m. Table 2.2 shows the condenser dimensions and materials

Parameters	Values
Condenser Length [m]	5.4
Inner Diameter [m]	0.007
Outer Diameter [m]	0.009
Curvature Diameter [m]	0.02
Fin Length [m]	0.2
Fin Width [m]	0.07
Fin Thickness [m]	0.001
Number of Fins	130
Space Between Two Fins [m]	0.0015
Number of Pipe in Pipe-Complex	20
Material	Copper
Fan Average Speed [m/s]	1.622

Table 2.2: Condenser dimensions and details

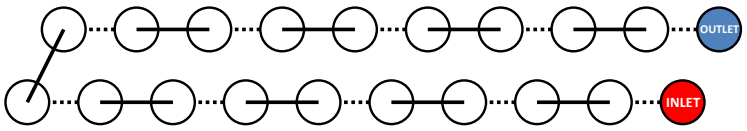

Figure 2.10: Condenser tubes-bank design

3. **Evaporator and Recuperator**

   In this work two brazed plate heat exchangers (PHE) from Alfa Laval Company are used as shown in Figure 2.11. One of them serves as the evaporator and connects to the TCB oil loop. The other one is used as a recuperator between the condenser and evaporator. PHEs are the most compact and better performing heat exchangers comparing to other traditional types. The work principle of the PHE is to exchange heat between two fluids without mixing them together by making the hot fluid flows in the even-numbered channels, while the cold fluid flows in an opposite directions in the odd-numbered channels as shown in Figure 2.12.

Figure 2.11: Plate Heat Exchanger

Corrugated stainless steel plates provide the heat transfer area. A compact 1kW brazed plate heat exchanger manufactured by Alfa Laval has been selected for the evaporator with dimensions of (21*7.4*1.1)cm. The total volume of the cold and hot side of the heat exchanger are 0.05 and 0.03 liter respectively with three channels for refrigerant-side and two channels for oil-side.

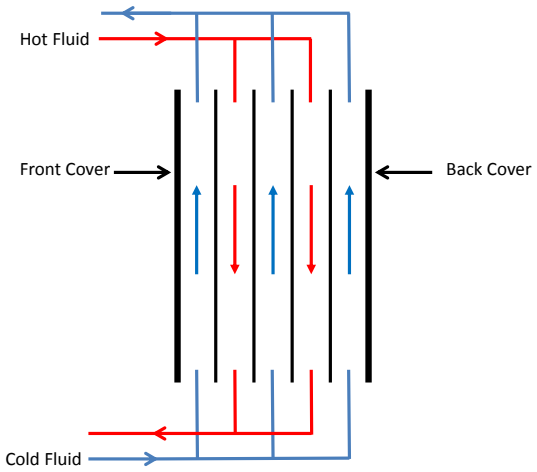

Figure 2.12: Plate Heat Exchanger Schematic Diagram

4. **Expansion Device**

The throttling device is the fourth main component in the refrigeration system that control the flow of the refrigerant in the VCC. It is a flow restricting device that forces the refrigerant to flow through a small cross sectional area channel, which cause a drop in the refrigerant pressure and temperature immediately after the restriction and before entering the evaporator. There are different types of expansion devices used in commercial air

conditioning systems. The main types are the capillary tubes and thermostatic expansion valves (TEV). The main disadvantage of the capillary tube is the fixed cross sectional area that the refrigerant will pass through. A metering device with variable opening position from Swagelok Company is used as an expansion or metering valve in this work as shown in Figure 2.13

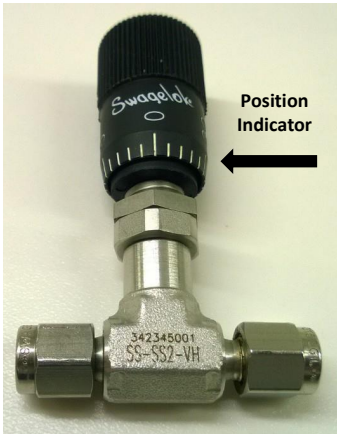

Figure 2.13: Metering valve with position indicator handle

2.2.2 Auxiliaries

1. **Mass Flow Meter**

   In order to measure the refrigerant flow rate in the main cycle and the TCB flow rate in the secondary cycle, two mass flow meters from General Electric Company are used. The flow meters are excited using a 24 VDC and has 4-20 mA signal output. They have a cut-off flow rate of 0.03% of the full capacity which is 18 g/min for the refrigerant flow meter and 180 g/min for the TCB flow meter. The flow meter calibration calculation provided from GE Company is mentioned in Table 2.3.

Flow Rate [g/min]	Error [%]
600	0.06
480	-0.10
240	0.14
120	-0.03
Experimental Data Range	
60	-0.05
30	-0.08
8	-0.26

Table 2.3: GE mass flow meter calibration data

2. **Filter Dryer**

The filter dryer has two essential functions. The first one is to remove water or humidity from the refrigerant. The second one is to provide physical filtration for any particles or foreign substances in the system that can harm the other components. A filter dryer from Schindler Company is used in the VCC test-bed setup.

3. **Temperature Control Bath**

The selected temperature control bath (TCB) contains a cooling system and a heating device connected to the main bath through a tube-bank heat exchanger and a heating cartridge respectively to maintain a precise fluid temperature. The TCB also contains a small internal pump with 6 speed steps. The pump can circulate the transport fluid inside the bath or circulate it through an external loop. The TCB has a built-in programming software that allows the user to set the bath temperature and program a specific scenario that maintain or change the fluid temperature at specific time period, select the pump speed and specify the acceptable temperature tolerance. The TCB has a wide range of temperatures from -120 to 250 °C and different fluids can be used. A silicone oil with properties given in Table 2.4 is used because it stays in liquid form in a range from -10 to 120 °C.

Description	**Data**
Supplier	Clearco Products Co., Inc
Chemical Name	Polydimethylsiloxane
CAS No	63148-62-9
Viscosity [cSt]	50
Specific Heat [cal/(g.C)]	0.36
HMIS Rating	
Health [0 to 4]	0
Flammability [0 to 4]	1
Reactivity [0 to 4]	0

Table 2.4: TCB Oil Specifications

4. **Measurement Devices**

A. **Thermocouples**

The bench setup contains 15 points to measure the temperatures. T type thermocouple probes from Omega Company are used. A basic calibration has been done using the TCB for a range from 0 to 85 ^{o}C. The uncertainty of the temperature measurement is around $\pm$ 1.7% of 1 °C. The probes are inserted through a double sealed plug and the tips are directly exposed to the fluid to measure the temperatures at the

inlet and exit of each component.

B. **Pressure Transducers**

The pressures at the inlet and exit of the compressor and expansion valves are measured using absolute pressure transducers from Omega Company. The transducers ranges are from 0 to 100, 200, 300, and 500 psi. The 100, 200, and 300 psi transducers are excited with 24 VDC, while the 500 psi transducer are excited with 10 VDC. They have accuracy up to $\pm$ 0.15% of full scale.

C. **Power Supply**

Three different power supplies are used to supply very precise VDC power to the bench setup. The first power supply is connected only to the compressor control unit. The compressor needs more current at the start up that could reach more than 2.5 A. This power supply has a range of (0-40)VDC and (0-4)A. The other power supply, from Agilent Company, is connected to the 500psi pressure transducer and excite it with 10 VDC. The last power supply, also from Agilent Company, is used to excite the other pressure transducers and the two mass flow meter with 24 VDC.

D. **Data Acquisition Unit**

In order to read the measurements from the bench setup, two different DAQs are used to receive all the signals from the mass flow meters, pressure transducers, and thermocouples. The first DAQ from National Instruments is designed specially to read thermocouples signals. Hence, all thermocouples probes are connected to this DAQ and the data is recorded using Lab View software. The other DAQ from Agilent company is designed to read current and voltage signals. Mass flow meters and pressure transducers are connected to this DAQ and the data is recorded through software provided by the same company.

E. **Air Velocity Measurement**

A Multi-function measuring Instrument from testo Company is used to measure the air velocity across the condenser. The device has been calibrated using a calibrated

wind tunnel. Figure 2.14 shows the calibration graph for testo instrument.

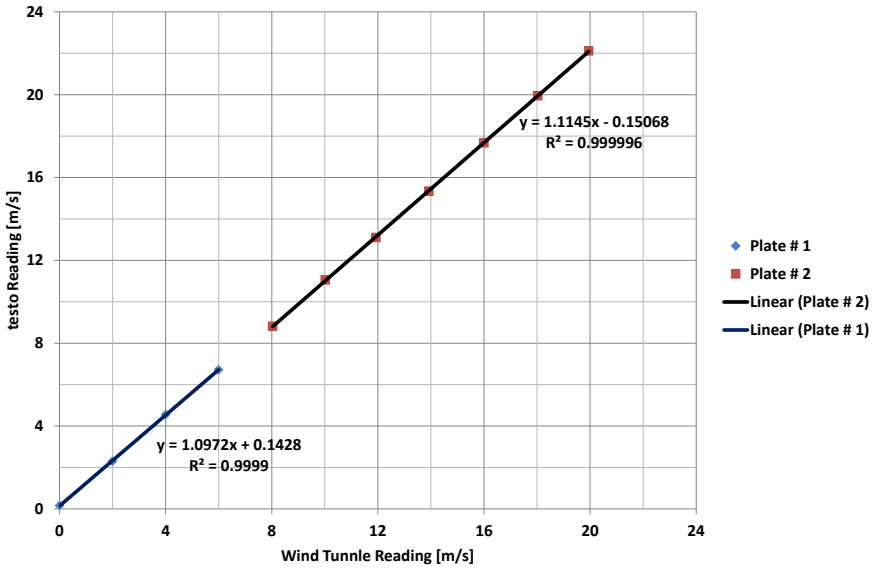

Figure 2.14: Air velocity instrument calibration curve

2.3 Construct VCC Test-Bed

2.3.1 Components Assembly

1. **Frame**

   The main objective of this work is to build a portable compact cooling system. Therefore, the whole cycle should be mounted together on the same frame. A (30 $\times$ 45 $\times$ 45) cm rectangular frame made of aluminum rails is constructed to carry the whole loop as shown in Figure 2.15.

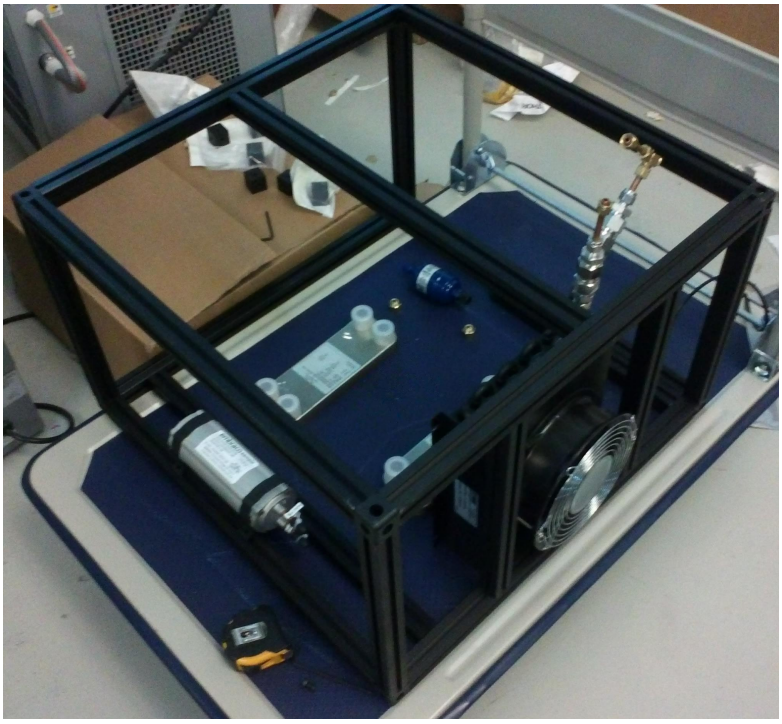

Figure 2.15: Parallelogram aluminum frame

2. **Components Positioning**

   The main challenge of building the test-bed is to convert the schematic diagram of the VCC (Figure 2.4) into a three dimension setup. Precise measurements of the components dimensions, the components order and the measurement device orientations should be taken into account before fixing the components in their final positions. Additionally, some manufacturer requirements restrict the components arrangement. For example, the mass flow meter manual mentioned that measuring module should be installed in a certain orientation to measure liquid mass flow rate, where the inlet and exit pipes should be in a higher position to prevent any gases to become trapped in the flow meter. Other restrictions could come from the operational needs. For instance, the flow in the PHE should be a counter-flow type as shown in Figure 2.12. In the recuperator case, the PHE is coming directly after the mass flow meter, as per the manufacturer recommendations, the pipe should rise directly after the exit connection. Hence, the liquid line from the mass flow meter to the PHE should be connected at the top inlet connection of PHE and leave from the bottom exit connection. Another example is the measurement devices orientation. Thermocouples probe should be reading the temperature at the inlet and exit of each component. Hence, the probe head should be as close as possible to the inlet and

exit points. Therefore, the T-connections should be oriented in different ways based on where they should read the temperature. Figure 2.16 illustrate the need for different probe orientations at different points.

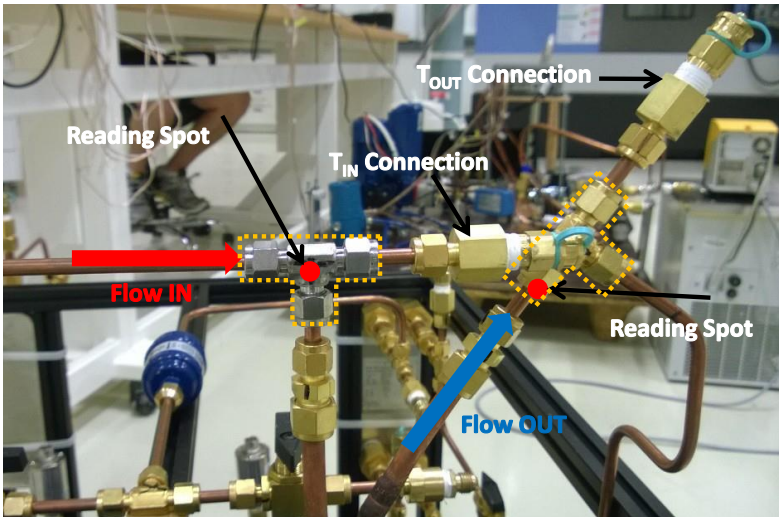

Figure 2.16: Different T-connection and thermocouple probe orientation at the inlet and exit of the condenser

The last important point about component positioning is the installation. The components should be installed in a rigid and fix position, so they will not be affected by any vibration caused by moving the bench, tightening some fittings, or any other reason that could cause the component to shake freely. Figure 2.17 gives an example of wrong installation. The PHE are tied to the frame by cable ties. A small vibration to the frame could cause a damage in the fittings and then cause an undesirable leakage. Also, the expansion valve is fixed by the pipe connection only. There is no other support to carry or handle it. This free installation will cause some stresses on the fittings which will create a potential for a leakage spot.

Figure 2.17: Wrong Installation for PHE and expansion valve

In contrast, Figure 2.18 shows better installation for the same equipment. The PHE is held between two aluminum rails, stand on two aluminum fittings, and tied by two cable ties. Also, the expansion valve is held by a simple stand from a 3/8 inch copper pipe piece. Both of the two components are now in a more stable positions.

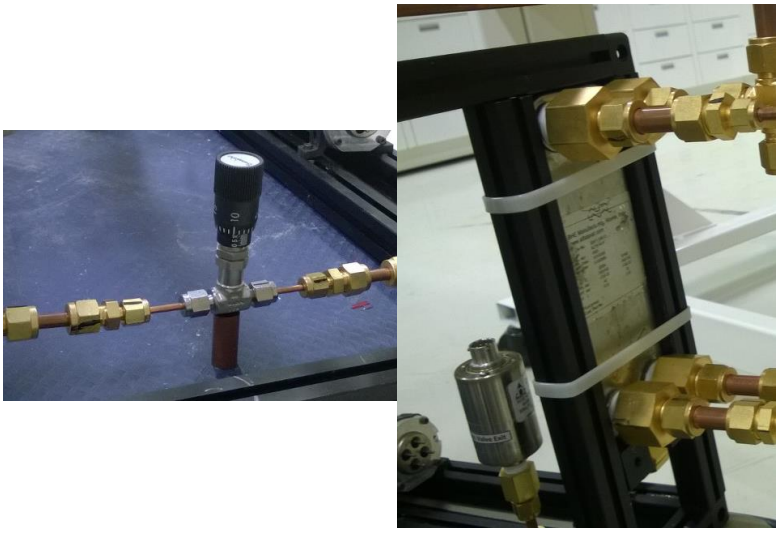

Figure 2.18: Correct Installation for two different components

3. **Components Connection**

   After placing the main components in their final position, accurate measurements should be taken for the distance between them. The VCC components are connected to each other using copper pipe and brass fittings. The main pipe size used in this work is 1/4" copper pipe. Other pipe sizes are used to connect the components with the main loop piping system. Copper pipe will be cut and bent based on the distance measurement to connect two components to each other. Special care must be taken in handling the copper pipes. The pipes come as 2 m pieces in a hardboard container. Based on the required length, the pipe is cut using pipe cutting equipment. A robust cutting tool should be used to have smooth cut and to prevent any residual after cutting the pipe. The cutting procedure should be done precisely and slowly. A fast cutting will lead to a deformation in the pipe and it will not fit in the fitting. A smooth and clean pipe end is required to prevent any leakage potential. Sand paper may not be used to remove any residual at the pipe end to reduce the pipe diameter and push it to fit in the gaugeable fitting. This procedure is one of the main reasons for having leakage at the fitting connection points.

   A pipe bender is used to bend the pipe precisely at the required place and with the required angle. A 5 mm difference could cause the pipe not to fit exactly at the center of the fitting. Forcing the pipe to fit in the fitting will cause a stress at one side of the ferrules and create a leakage potential. It is recommended to use softer copper pipes for the sizes from 1/2"

and above. Bending thick copper pipes is not an easy procedure and it most likely end up with a broken bend.

Three different fitting types are used in connecting the equipment as shown in Figure 2.19.

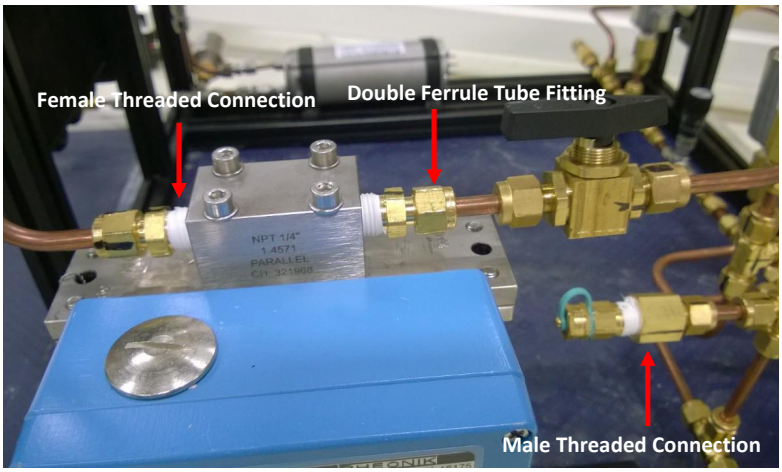

Figure 2.19: Different fitting types are used in building the test-bed

The first one is threaded male/female connection. The other type is Flare connection and it is used only to connect the filter dryer. The third one is the gaugeable tube fitting type which is commonly used in this work. Figure 2.20 shows the different fittings that used in building the test-bed.

Figure 2.20: Tube fittings (a) gaugeable tube fitting with double ferrule. (b) male threaded fitting (c) female threaded fitting (d) flare type fitting for filter dryer. Source (www.swagelok.com)

Choosing proper fittings is one of the most important steps in building any bench setup. Improper fittings will lead to a big leakage potential. Welded fittings are the best choice but require an expert to do the welding. Also, once the system is set up it will not be easy to modify any connection or arrangement. Hence, the gaugeable tube fittings along with threaded fittings are the most suitable choice for experimental test-beds. There are different types of the gaugeable tube fitting. The common used one is that type with single ferrule as shown in Figure 2.21.

Figure 2.21: Gaugeable tube fitting with single ferrule. Source (www.brennaninc.com)

This type is cheaper than the double ferrule type and more available. It has a single point to swage the pipe, while the double ferrule fittings has two points of swaging which means better sealing.

4. **Tightening Procedure**

   There are different procedures for tightening the fittings based on the fitting type. For threaded male/female fittings, the thread is sealed by PTFE tape. More tape does not mean better sealing. The first line of the thread should not be covered by the tape. Also, 3-4 turns of the tape is enough. If PTFE tape is wider than the thread, then 2-3 turns is enough. The tape is used only to enhance the metal-to-metal connection between the male and female threads. Nevertheless, the threads should be in a good contact with each other to create better sealing. The next step is to tighten the connection. There is no role of thumb for such tightening, but enough torque should be given to secure the connection between the threads.

   The second type is the flare connection. PTFE tape is not needed for tightening this connection even it is a threaded type connection. Flare connection is based on flaring the tube using flare tool which consists of a die to hold the pipe and a mandrel that is forced into the end of the pipe to form the flare. The flare nut should be installed before gripping the pipe into the die. A 45 and 37 degree flaring styles are standard in such connection. Then use a spanner to tight the flared pipe with the flare connection (Figure 2.20d).

   Most of the fittings used in this work are double ferrule fittings. They are connecting

different pipe diameters through reducers. Also, they connect the pressure transducers and the temperature thermocouples sets to the loop through T-connections. Although the loop contains different sizes and type of the double ferrule fittings, the tightening procedure for this type is almost the same.

1. The pipe should be cut smoothly, bent correctly and inserted to the fitting without any extra force or push.
2. Loosen the fitting nut to allow the pipe to be seated against the shoulder inside the fitting body freely.
3. Be sure that the fitting has the two ferrules (Figure 2.20a).
4. Insure that the pipe is fully inserted to the fitting against the shoulder and then rotate the nut finger-tight.
5. Mark the nut and fitting body with a straight line using a marker.
6. Hold the fitting body using any suitable tool and then tight the nut one and one-quarter turns.
7. For pipe sizes smaller than 1/4", three-quarter turn is enough to tighten the tube.

The above steps should be followed carefully. If the pipe is not seated against the shoulder, the metal-to-metal connection between the swaged pipe and the fitting is not enough. Also, more tight does not necessarily mean better sealing. However, less tightening means more leakage potential.

5. **Final Assembly**

   After connecting the pipes to the VCC components and to the measurement devices, the loop should be assembled to together into the final shape. Choose a suitable point to start from, follow the tightening procedure (point 4) and the bench test-bed is ready for the next step as shown in Figure 2.22.

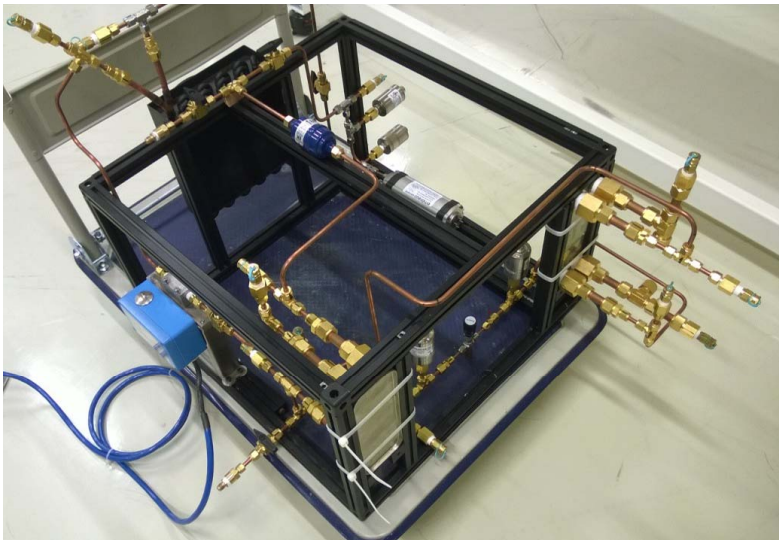

Figure 2.22: Assembled compact VCC test-bed

2.3.2 Leakage Test

Once the loop is assembled it has to be tested for leakage. The first step is charging the loop through the charging valve with nitrogen to a pressure of 900 to 1000 kPa. After that the charging/discharging valves closed and the leakage test begins. The loop is now isolated, the four pressure transducers are connected to the DAQ to read the pressure inside the loop from four different points. Since the pressure inside the loop is equalized, the pressure transducers should measure the same pressure value. At the same time a soap-water solution is used to paint all the fitting connections to check if there is any leakage. Nitrogen will escape from the points that have leakage creating small bubbles. All leakage spots should be tightened and the procedure should be repeated until all leakage spots are fixed. In parallel the DAQ should read the pressure for 24 hour, if the pressure reading reduced, then the loop still has leakage and should be tackled.

Leakage test could stay for months, or could be done in three days. The first test-bed setup was built with no experience in building loops. Figure 2.23 shows the old and new test-bed and highlights the differences between them.

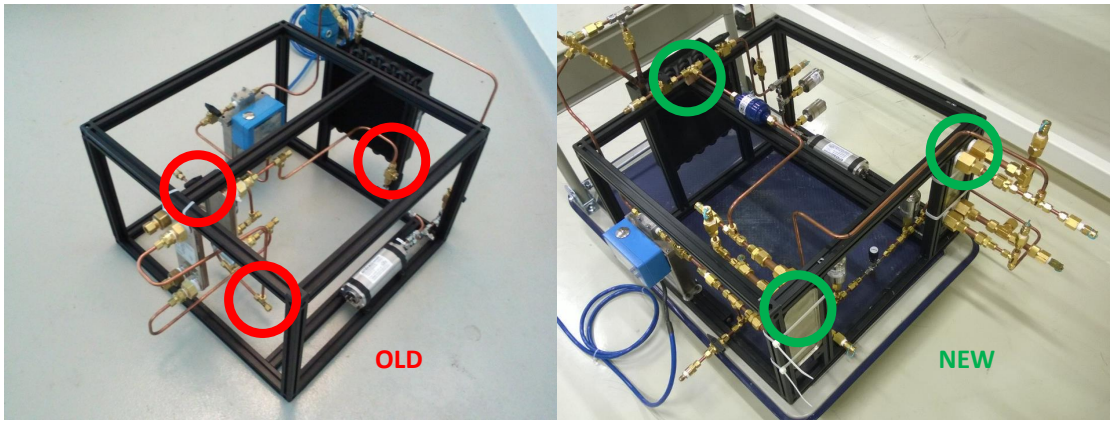

Figure 2.23: The first and second test-beds

The guidance mentioned before about pipe handling, fittings selection and fittings tightening were missed in the first test-bed. The first leakage condition persisted for six months and was impossible to stop. Many reasons were behind the leakage in the first test-bed including:

1. Using improper fittings with single ferrule.
2. Tightening the fittings as much as possible.
3. Wrong equipment positioning and installation (Figure 2.17)
4. Using a low quality pipe cutter that caused a lot of residual after cutting the pipe
5. Wrong cutting procedure. The cut was fast, and the cutting tool was pushed to cut the pipe in fewer turns.
6. Sanding the pipes with a sand paper to remove the residuals and reduce the diameter to push the valve to enter the fittings ferrules
7. Force the pipes to enter the fittings if the bending was imperfect and shifted 3-5 mm.
8. When the first loop disassembled, most of the pipes were not seated properly in the fittings - the pipes did not reach the shoulder of the fittings.

The second test-bed setup was built by following the guides mentioned in the previous sections and with accurate and careful steps. There was only one leakage spot in the second test-bed through the recuperator thread and it was eliminated by tightening. The VCC is now sealed and ready for the next step.

2.3.3 Insulation

A rubber foam insulation material is used to insulate the loop. A 1/4", 3/8" and 1/2" insulation robes are used to insulate the loop pipes. Separate sheets from the same material are used to insulate different components and areas. Figure 2.24 shows the loop after the insulation.

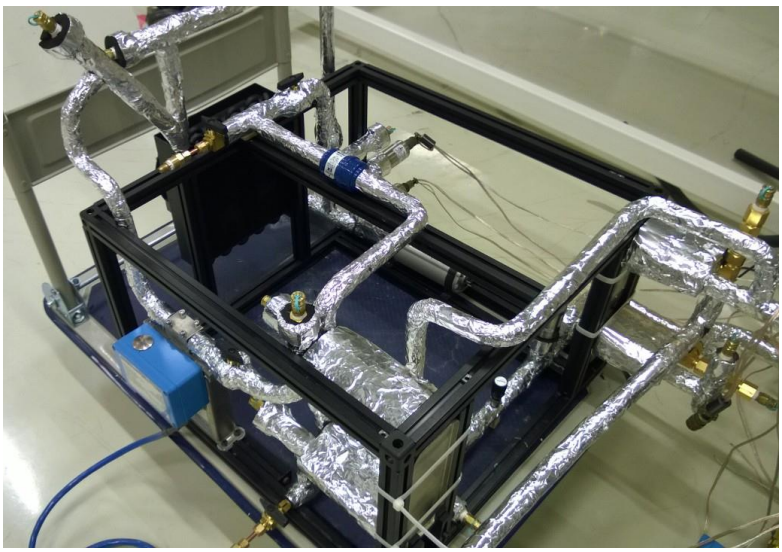

Figure 2.24: The VCC after insulation

After running the loop, the recorded data was showing temperatures difference between two consecutive points due to heat loss. For example, for starting up the loop, TCB temperature was set at 50 °C to heat up the refrigerant in the loop through the evaporator. The oil arrived at the evaporator inlet 5-6 °C lower than the TCB reading. Another example, the expansion valve exit temperature was reading -5 °C while the next point reading at the evaporator inlet was 5 °C. Hence, the loop was insulated again with better insulating material. Glass wool insulation was chosen to insulate the loop. Because of its extremely low heat transfer coefficient (0.03 W/mK at 0 °C and 0.04 W/mK at 75 °C), it was able to keep the oil temperature at the evaporator inlet as same as the TCB reading. Also, the expansion valve exit and the evaporator inlet thermocouples were reading the same temperature values. This insulation is applied to the whole loop.

2.3.4 Refrigerant Charging

The last step before start running the loop is charging the refrigerant. The loop will run first with R134a refrigerant. After that propane gas R290 will be used as a working fluid in the VCC test-bed. The first step is to evacuate the loop. A vacuum pump is connected through a charging hose set up to service ports at the high and low sides of the loop. Having two service ports will

ease the vacuuming procedure. The main goal of vacuuming the loop is to remove all foreign gases and small residuals in addition to boil-off any water that may still be in the loop. After two hours, the entire loop became under vacuum and ready to be charged by the refrigerant.

The vacuum pump and charging hose set up are connected to the refrigerant cylinder in such a way that all hoses are evacuated as shown in Figure 2.25.

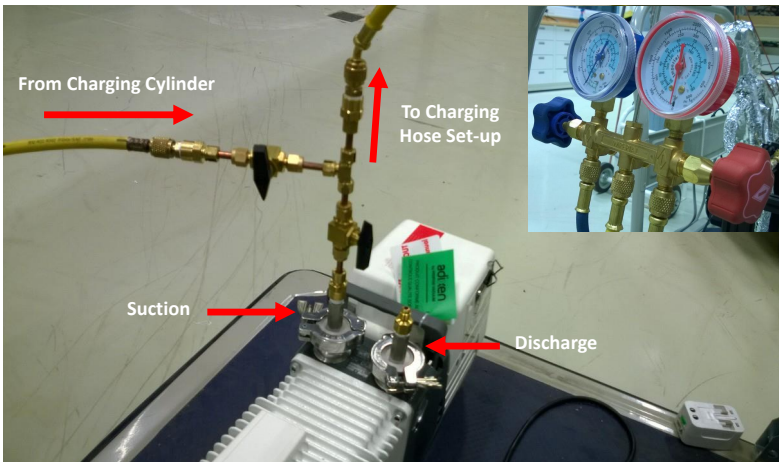

Figure 2.25: Vacuum pump connection set up

Before charging the gas, the amount of charge should be calculated. The performance of the VCC is related to the refrigerant mass in the loop [58]. The total volume of the loop has been estimated as mentioned in Table 2.5

Item	Volume [L]
Condenser	0.208
Evaporator	0.05
Recuperator	0.08
Pipe	0.1
Compressor	0.000267
Total	0.438

Table 2.5: VCC components volume

The pipe volume is estimated based on the diameter and the length of the consumed pipes in addition to fittings dimension. After that, the refrigerant mass has been calculated base on the expected pressure in the loop, the refrigerant phase and its associated density. The estimated mass of refrigerant that should be charged was calculated to be around 300 g.

A scale of tolerance $\pm$ 10 g is used to weigh R134a cylinder and the amount of charge. At the

beginning of charging R134a, the pressure difference between the cylinder and the vacuumed loop is enough to allow the refrigerant to liquefy into the loop. After certain point, the pressure difference will not be enough to charge more refrigeratn. In order to increase the pressure difference between the loop and the cylinder, the TCB temperature is reduced to 0 °C which will reduce the temperature and then pressure inside the evaporator. After that, the pressure inside will equalize into lower pressure which allow more refrigerant to flow into the loop.

The charging should be done only through the charging port at the loop low pressure side. After charging the desired amount of refrigerant, the charging port is closed and the test-bed is ready to run.

Chapter 3

VCC Experimental Characterization

3.1 Experiment Start-Up Procedure

After charging the loop and closing the charging valves, the loop is ready to be tested. The below procedure has been followed to start-up the loop.

1. Check the compressor, pressure transducers, flow meters, and thermocuples connections to the assigned DAQs and power supplies.
2. Turn the power supplies on and set the voltage limit to the required values.
3. Turn the voltage output on to excite the measurement devices and the compressor with the required DC voltages.
4. Turn the DAQs on and start up the softwares.
5. Set the DAQs scan time of recording data to the desired values. For this work a 2 sec. scan time is used.
6. Keep the system at its initial state for certain time to be sure that all readings are stable and to use them as reference state.
7. Set the TCB at high temperature (for example 50 °C) and the pump at maximum speed. Then, turn the pump position to the external flow and start the TCB. This step is important to increase the refrigerant temperature in the evaporator and then in the loop. This will prevent any liquid refrigerant to enter the compressor.

8. Open the expansion valve to its maximum opening position to minimize the pressure drop across the valve and allow more cold refrigerant to pass and mix with the hot refrigerant from evaporator.

9. Check the temperature and pressure at the compressor inlet. Using Refprop program, the refrigerant state can be calculated.

10. If the refrigerant at the compressor inlet becomes superheated,this means the loop is ready to start the operation.

11. Set TCB at the desired temperature and reduce the expansion valve position to the required opening.

12. Turn the compressor on using the software that is provided from Embraco Company. The program has the capability to run the compressor at different capacity (0-100)%. Start the compressor gradually from 10% to 20% and so on, to prevent any undesirable shock or damage in the compressor or in the loop.

3.2 Parametric Studies

Parametric study is a procedure that is followed to study the effect of changing one parameter in an experiment on the other components and whole cycle. This section will discuss the effect of changing the compressor capacity and the TCB temperature at different expansion valve opening position on the evaporator cooling capacity, cycle COP, pressure ratio across the compressor, condensation and evaporation temperature, and cooling load at the evaporator which is the amount of heat that is removed from the oil.

Different parametric studies are handled in this research. Linear compressor can run at different capacities, TCB can operate at different temperatures, and expansion valve has different opening positions. Changing these components operating conditions leads to different state and rates of compressor and evaporator energy input, recuperator heat exchange rate and condenser heat rejection rate. Table 3.1 shows the experimental plan for these parametric studies.

Experiment No.	Expansion Valve Position	TCB Temperature [°C]	Compressor Capacity [%]
1	4	25	(50 to 100) (10% step)
2	5	25	(50 to 100) (10% step)
3	6	25	(50 to 100) (10% step)
4	4	(10 to 25) (5 °C step)	90
5	5	(10 to 25) (5 °C step)	90
6	6	(10 to 25) (5 °C step)	90

Table 3.1: Parametric study experimental plan

At each step, the loop runs until steady state is achieved. For the first set of experiments the the TCB was set at 25 °C while the expansion valve open position changed from position 4 to position 6. At each position for the expansion valve, The compressor capacity started at 50% for 30 min. After that the capacity was increased by 10% each time until it reached the 100%. Figure 3.1 shows the pressure readings for the whole experiment. While Figure 3.2 depicts the temperature changes during the first parametric study.

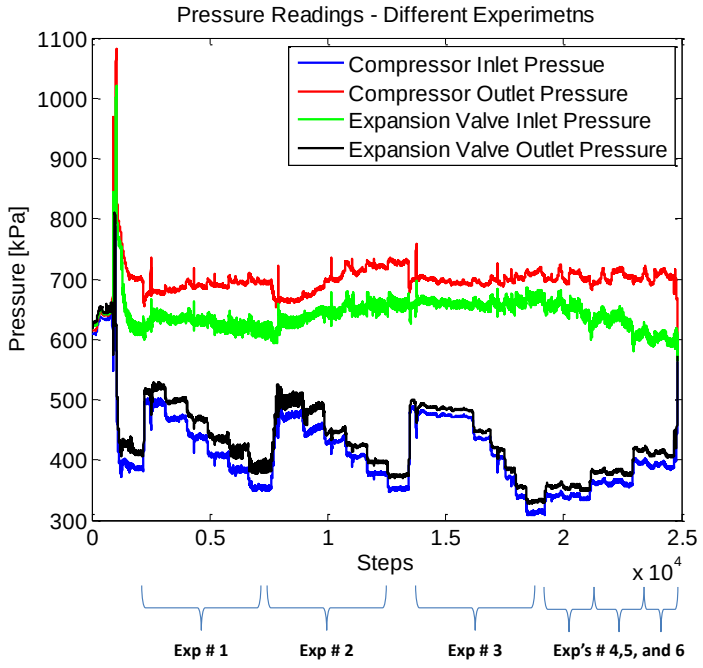

Figure 3.1: Pressure readings at different parametric studies

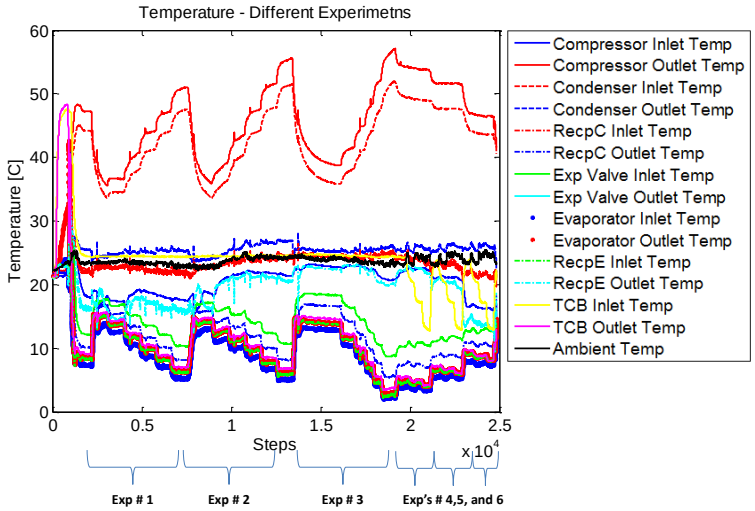

Figure 3.2: Temperature readings at different parametric studies

In the second set of experiments the compressor capacity was fixed at 90%, the expansion valve position changed from 4 to 6 and the temperature was changed from 10 °C till reach 25°C. Each step was held for 15 min and the step change was 5°C each time. Although the line between the TCB and the evaporator inlet was insulated very will, the oil temperature reached the evaporator (1-6.7) °C higher than the TCB readings. Table 3.2 summarizes the temperature differences between the TCB and the evaporator inlet.

TCB Temperature [°C]	Evaporator Inlet Temperature [°C]
25	+ 1 °C
20	+ 1.6 °C
15	+ 2.5 °C
10	+ 3 °C

Table 3.2: Oil temperature difference between TCB and evaporator at different points. Ambient temperature is 26 °C

3.2.1 Base Point Operation

As mentioned in Table 3.1 the test-bed has three parameters that can be adjusted. Changing these parameters gives 30 different cases. In order to study and understand the effect of changing these parameters on the VCC performance and the components efficiencies, the system should reach a steady state scenario in each case. The test-bed ran each case for 15 to 30 min. This time period was enough to allow the system to closely approach the steady state operation. After that, the parameter changed to the next case as shown in Figures 3.1 and 3.2. In the all parametric studies, the system starts from the same base point. The base point was set at 90% compressor capacity,

25 °C TCB temperature, and open position 4 for the Expansion valve. Figure 3.3 Shows the steady state temperature, pressure, and mass flow rates at the selected base points.

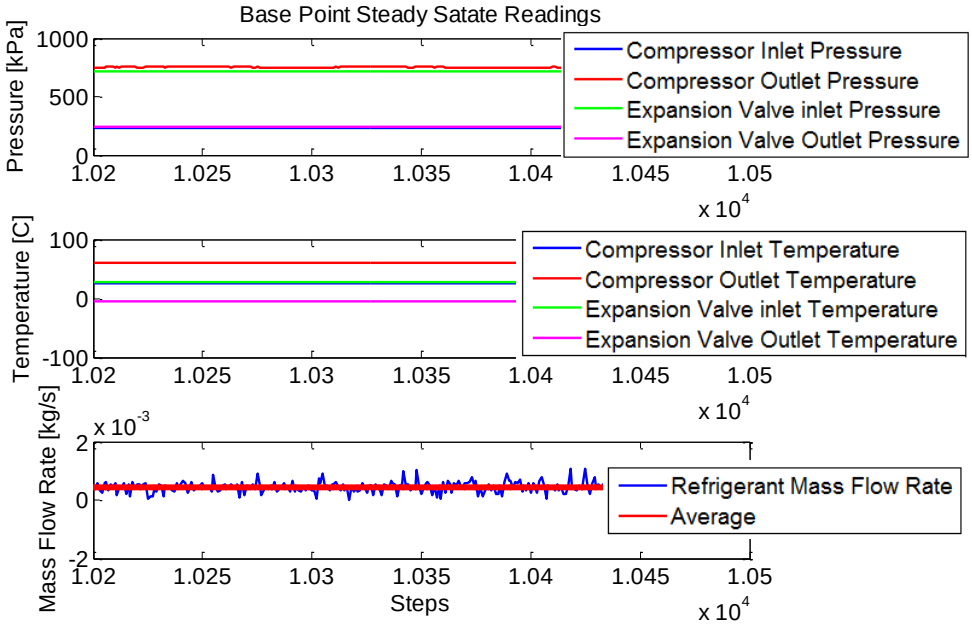

Figure 3.3: Base point steady state readings

3.2.2 Changing Compressor Capacity

The compressor is the only moving part in any refrigeration or air conditioning systems. It is one of two components that causes the pressure difference in the cycle. Compressor operation is controlled through a program that is provided from the manufacturer Embraco Company.

Linear compressor capacity indicates how much the piston is moving away from the top dead center (TDC). Figures 3.4 and 3.5 show the P-h and T-s diagram of the VCC for different compressor capacities at expansion valve open 6.

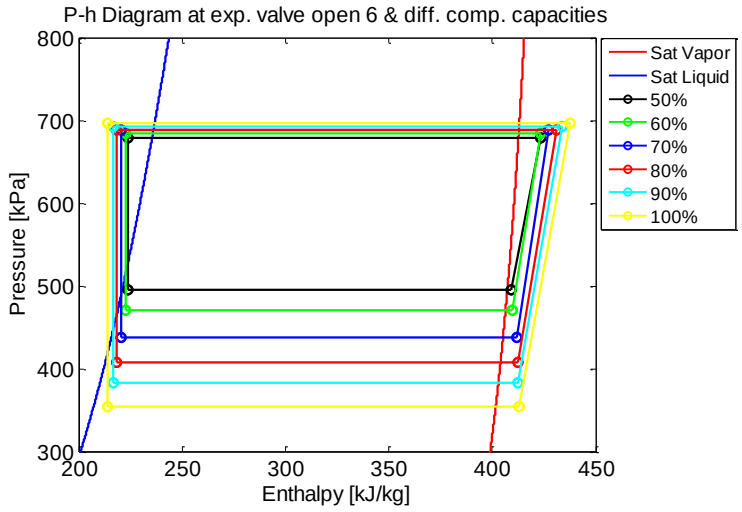

Figure 3.4: P-h diagram for the VCC test-bed at different compressor capacities

Pressure ratio across the compressor is defined by Equation 3.1 which increases with increasing the compressor capacity for a given ambient temperature, condenser fan speed, and TCB temperature.

$$PR = \frac{P_{out}}{P_{in}} \tag{3.1}$$

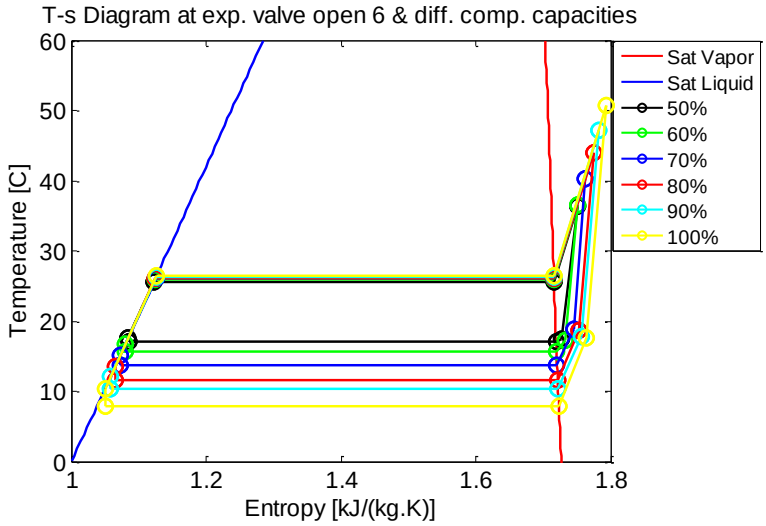

Figure 3.5: T-s diagram for the VCC test-bed at different compressor capacities

Figure 3.6 shows the pressure ratio at different compressor capacities and expansion valve opening positions. When the compressor capacity increases at same expansion valve opening position, the pressure ratio across the compressor increases since the only changing parameter is the compressor capacity. Now, when the expansion valve opening position changes from four

to six, the cross sectional area of the valve increases which leads to lower pressure drop across the valve. Therefore, the pressure ratio across the compressor decreases when expansion valve opening position increases.

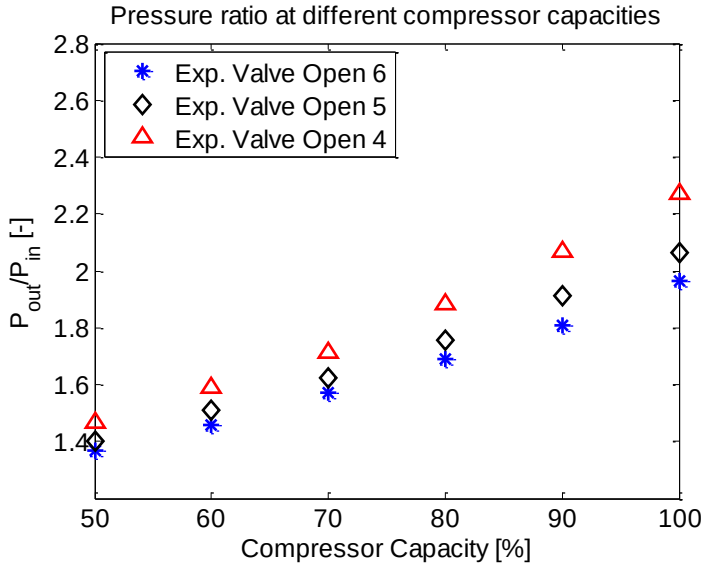

Figure 3.6: Pressure ratio across the compressor at different capacities

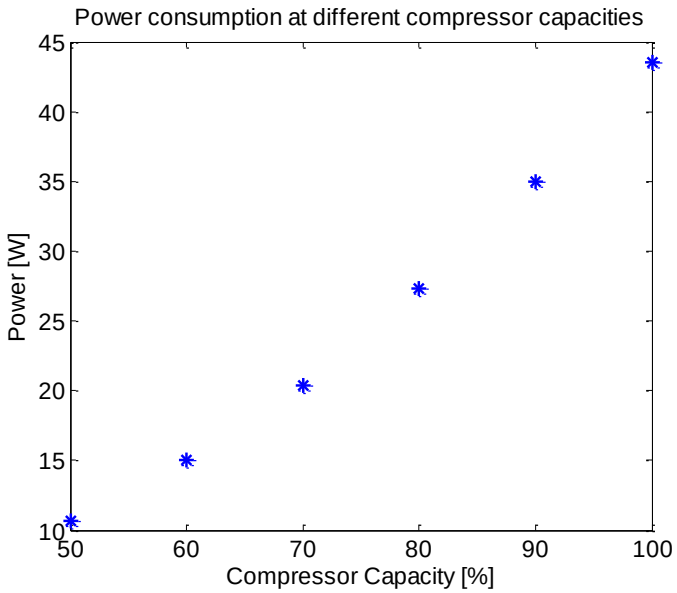

Figure 3.7: Compressor power consumption at different capacities

The coefficient of performance (COP) is defined by Equation 2.1. When the compressor capacity increases both the compressor power consumption and cooling capacity increase as shown in Figures 3.7 and 3.11.

However, the increase in the power consumption is higher than the increase in cooling capacity. Hence, COP of the cycle decreases as compressor capacity increases as shown in Figure 3.8.

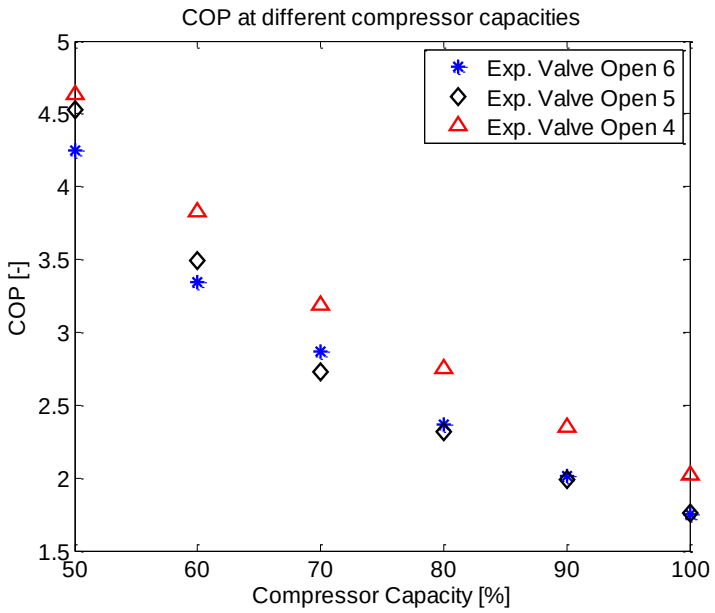

Figure 3.8: Coefficient of performance at different compressor capacities

Figure 3.9 shows the effect of increasing the compressor capacity on the condensation temperature. When the compressor capacity increases, the exit pressure and temperature are also increase. Compressor modeling in Appendix A discusses the relation between increasing the piston stroke length and increasing the exit pressure and temperature.

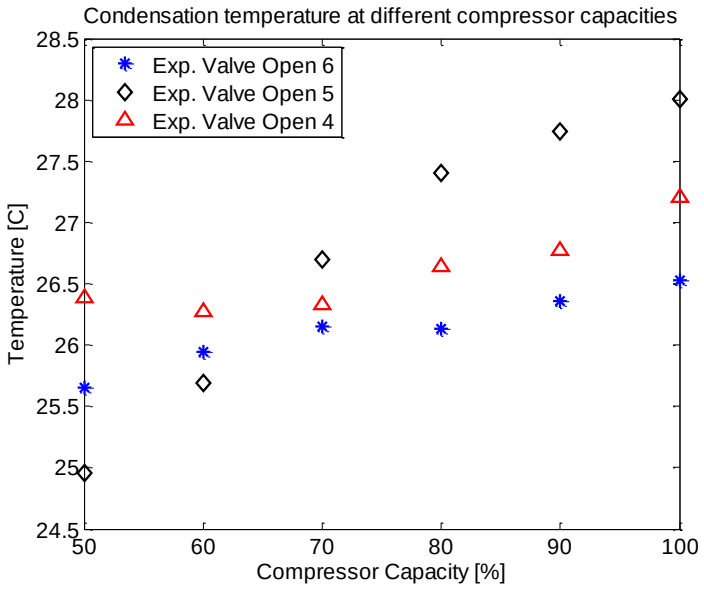

Figure 3.9: Condensation temperature increases with increasing the compressor capacity

As discussed in Figure 3.6, the pressure difference across the compressor increases with increasing the compressor capacity. This increase affects the pressure difference across the expansion valve. The pressure at the expansion valve inlet is almost the same as the compressor exit. Also, the expansion valve opening position is fixed. Hence, when the pressure ratio increases the exit pressure of expansion valve will decrease and this will affects the refrigeration temperature that will enter the evaporator. Figure 3.10 shows the relation between the compressor capacity and evaporation temperature. The effect of the pressure ratio across the compressor and the pressure difference across the expansion valve leads to reduce the evaporation temperature when the compressor capacity increases.

As the refrigerant passes through the evaporator, it gains heat from the transport fluid which leads to evaporation of the refrigerant. The amount of heat removed at the evaporator is called cooling capacity and is defined as below:

$$\dot{Q}_c = \dot{m}\Delta h \tag{3.2}$$

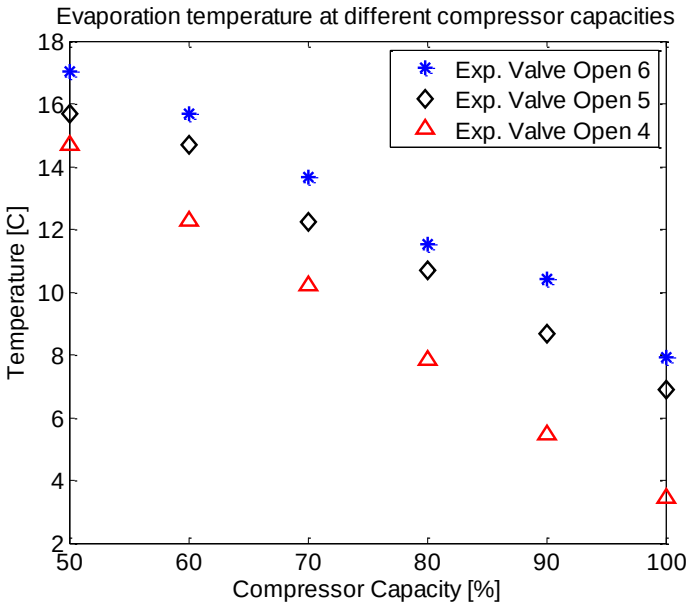

Figure 3.10: Evaporation temperature decreases with increasing the compressor capacity

The increase in compressor capacity leads to a lower pressure and temperature at the expansion valve exit. This means the temperature difference between the refrigerant and the oil will increase which leads to increasing in the cooling capacity as shown in Figure 3.11. Also, decreasing the expansion valve opening position at the same compressor capacity leads to a lower pressure and temperature at the valve exit which means more temperature difference between oil and refrigerant.

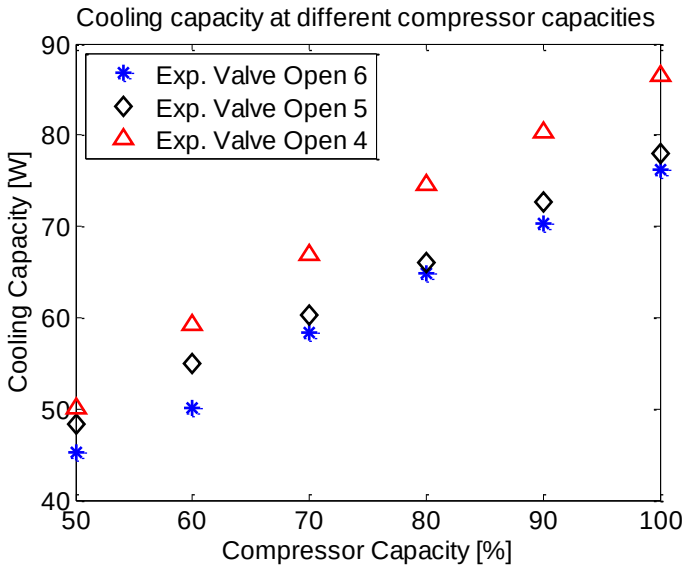

Figure 3.11: The effect of increasing the compressor capacity on the evaporator cooling capacity

3.2.3 Changing TCB Temperature

The temperature control bath described in Chapter 2, is used as a heat sink to simulate a cooling load. The working fluid specifications are mentioned in Table 2.4. Fluid viscosity and density change with temperature and the oil that is used in this work showed a normal trend for flow rate against TCB temperature changing as shown in Figure 3.12. This change in flow rate is affecting the heat transfer rate between oil and refrigerant at evaporator according to Equation 3.3. The increase in mass flow rate will increase the heat transfer rate to the refrigerant. Figure 3.13 shows the increase in the cooling capacity at evaporator with increasing the TCB temperature.

$$\dot{Q} = \dot{m} C_P \Delta T \tag{3.3}$$

Where C_P is the specific heat of oil and it is assumed to be constant over the TCB temperature change range.

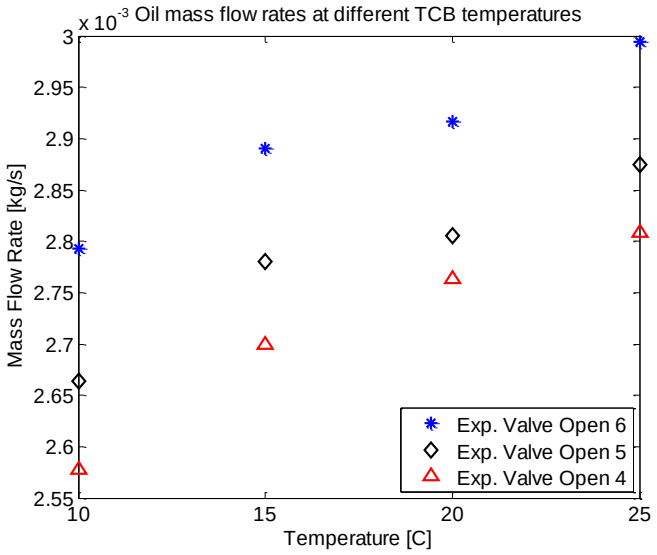

Figure 3.12: Oil mass flow rate increases with increasing the TCB temperature

Also, the logarithmic mean temperature difference (LMTD) between the refrigerant and oil is higher at higher TCB temperature, which will increase the heat transfer in the plate heat exchanger (evaporator).

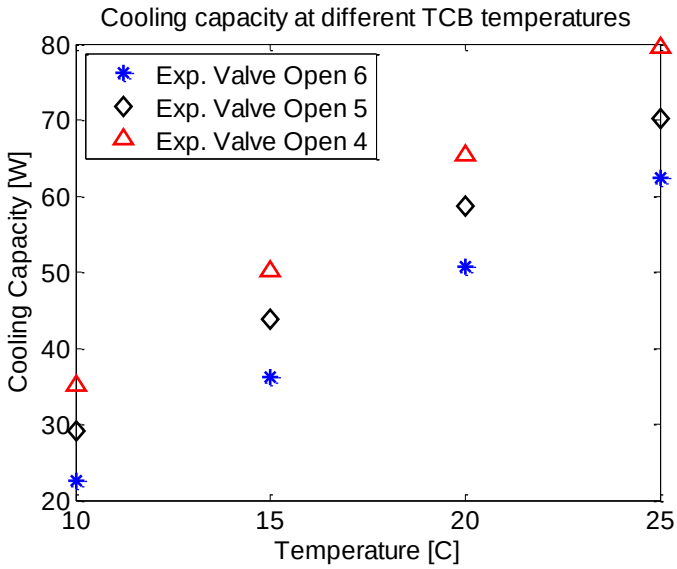

Figure 3.13: The effect of increase TCB temperature on the cooling capacity

$$LMTD = \frac{\Delta T_R - \Delta T_O}{ln\left(\frac{\Delta T_R}{\Delta T_O}\right)} \tag{3.4}$$

Where ΔT_R is the difference between the refrigerant temperatures at evaporator inlet and exit. ΔT_O is the oil temperature difference between evaporator inlet and exit.

$$\dot{Q} = U \times A \times LMTD \tag{3.5}$$

Where U is the heat transfer coefficient$[W/(m^2K)]$ and A is the exchange area $[m^2]$.

The increase in cooling capacity at fixed power consumption will increase COP as shown in Figure 3.14.

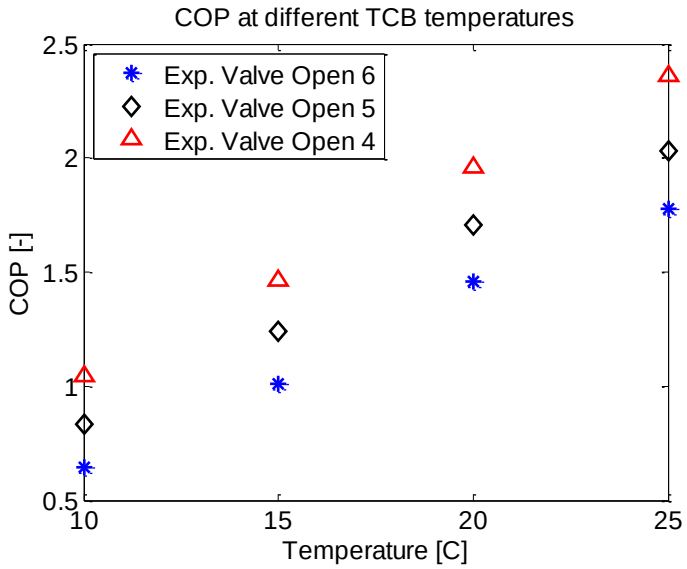

Figure 3.14: COP increases with increasing the TCB temperature at fixed compressor capacity

Figures 3.15 and 3.16 shows the P-h and T-s diagrams for the VCC at different TCB temperature. It is clearly shown that changing the TCB temperature has small effect on the condensation temperature, evaporation temperature, and pressure ratio across the compressor due to the small mass flow rate of the oil.

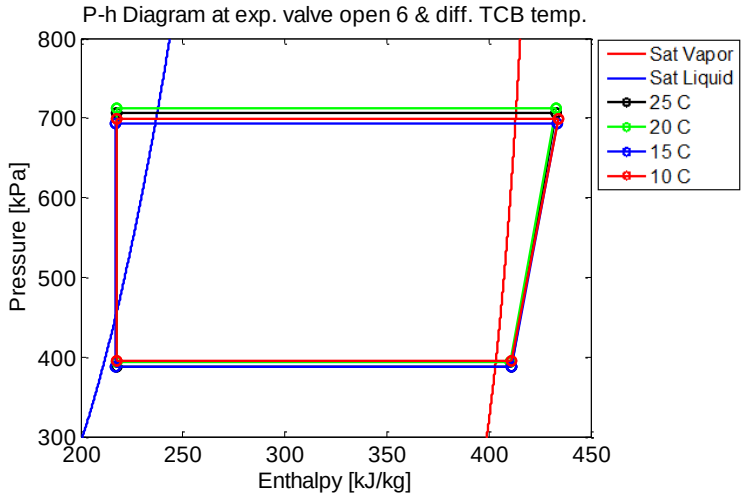

Figure 3.15: P-h diagram for the VCC test-bed at different TCB temperatures

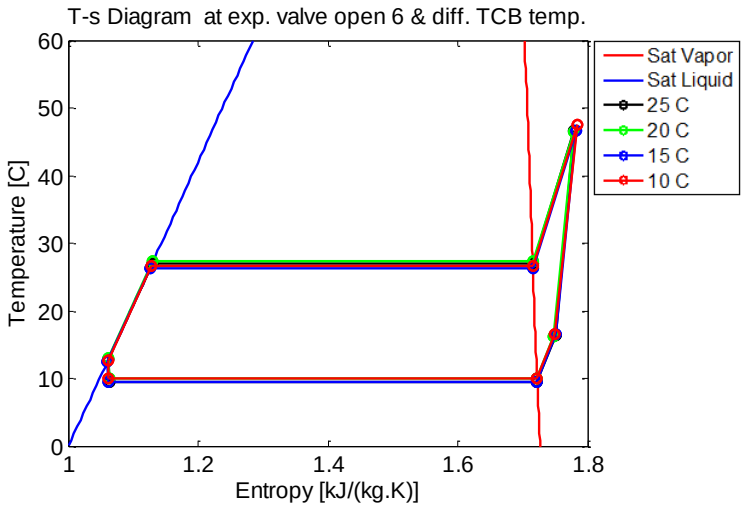

Figure 3.16: T-s diagram for the VCC test-bed at different TCB temperatures

The pressure uncertainty is given in Chapter 2. The uncertainty in the enthalpy calculation is obtained based on the pressure transducer and thermocouples that mentioned the same chapter. At evaporator outlet point, the refrigerant exit as a two-phase flow. A heat balance between oil side and refrigerant side is carried out considering the heat gain from ambient (mentioned in Section 4.1.5). The enthalpy at evaporator outlet is then calculated based on equation $Q = \dot{m}\Delta h$. The uncertainties of mass flow meters (for oil and refrigerant), thermocouples and pressure transducer are used to calculate the uncertainty of the enthalpy at evaporator exit.

Figure 3.17 shows the energy balance check for evaporator and the whole system which lie within $\pm$ 5% error margin. The heat transfer in evaporator is between the TCB oil and refrigerant.

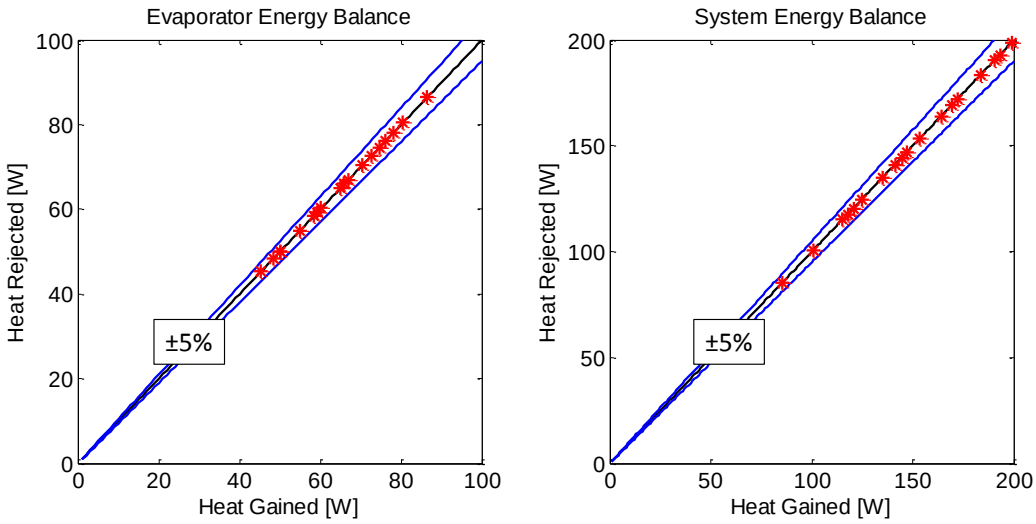

Figure 3.17: Energy balance check

3.2.4 Effect of Changing Expansion Valve Open Position

The expansion valve is a device controls the amount of refrigerant passed into the evaporator by reducing the flow cross section area. The restricted area causes a sudden reduction in refrigerant pressure and temperature which is called throttling. The expansion valve used in this work is a metering valve from Swagelok Company with dimensions mentioned in Figure 4.5.

The expansion valve is controlling the refrigerant mass flow rate. So, when the valve opening position increases the cross sectional area will increase which means more mass flow rate as shown in Equation 3.6.

$$\dot{m} = \rho \times u \times A \tag{3.6}$$

where u is the refrigerant velocity $[m/s]$ and A is expansion valve cross sectional area $[m^2]$.

When the valve open position increases, the valve needle rises up which increases the flow cross section area. The increase of area will then decrease the pressure drop across the valve. This mean that the pressure ratio across the compressor will be lower.

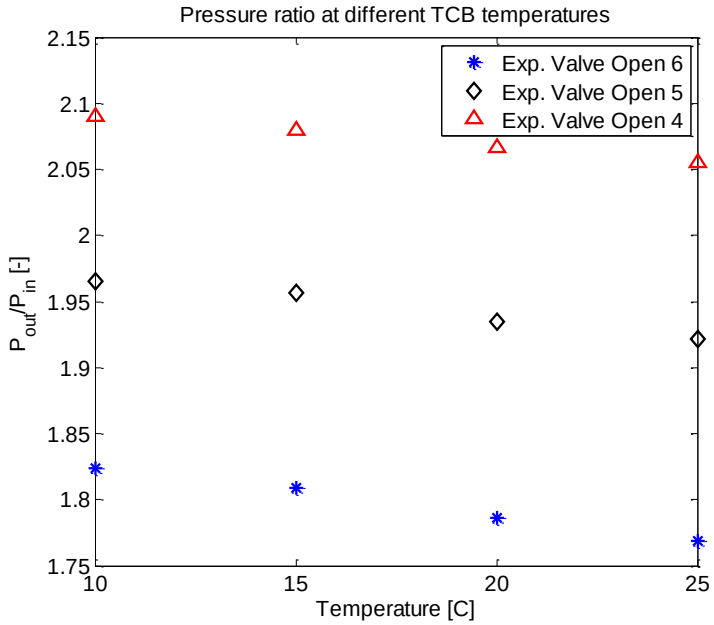

Figure 3.18: Pressure ratio across the compressor at different TCB temperatures

Figures 3.6 and 3.18 show the effect of increasing the valve open on decreasing the pressure ratio across the compressor at fixed compressor capacity and TCB temperature.

Pressure drop in the expansion valve becomes lower with increasing the valve open. This trend will increase the evaporation temperature and then reducing the evaporator cooling capacity as discussed before and shown in Figures 3.10, 3.11 and 3.13. Additionally, COP of the system decreases when expansion valve open position increases since compressor capacity is fixed and cooling capacity is decreasing as shown in Figures 3.8 and 3.14

Next section will discuss the effect of operating the system at this optimum situation on the heat transfer in evaporator, recuperator operation, and lowering the pressure ratio across the compressor.

3.2.5 Recuperator Effect

In the proposed configuration in Chapter 2 a recuperator is introduced to utilize the temperature difference between the condenser and evaporator. Recuperator heat load is then related directly to the condensation and evaporation temperature which in term are related to the cycle operation condition.

As discussed before, condensation temperature increases and evaporation temperature decreases with increasing the compressor capacity. The increase in the temperature difference between condenser and evaporator will increase the heat transfer in the recuperator as shown in Figure 3.19.

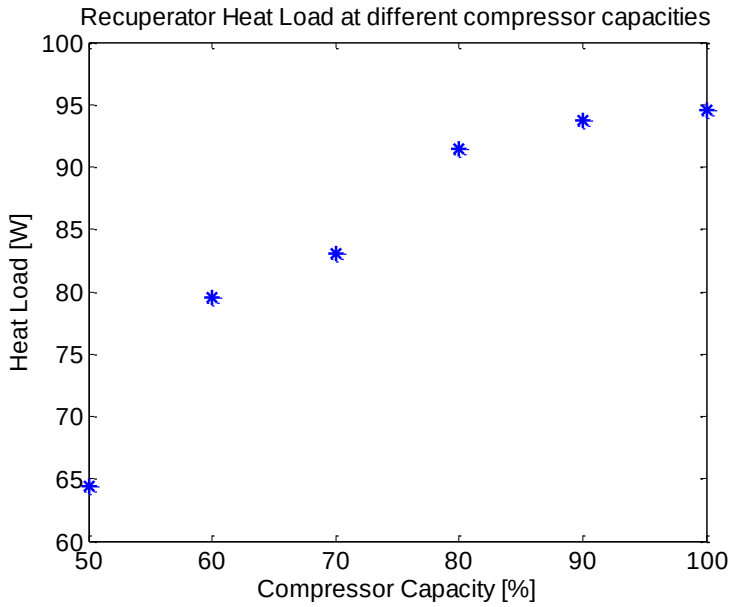

Figure 3.19: Recuperator heat load increases with increasing compressor capacity

3.3 Efficient Operation Point

As discussed in the previous section, the system shows a better performance at specific operation point. In general better system performance means better COP, but for the proposed configuration in this work choosing the highest COP operation point is not enough to select the most efficient operation point.

Figure 3.20 shows the amount of super-heated and sub-cooled degrees that recuperator adds to the refrigerant before the compressor inlet and after condenser outlet.

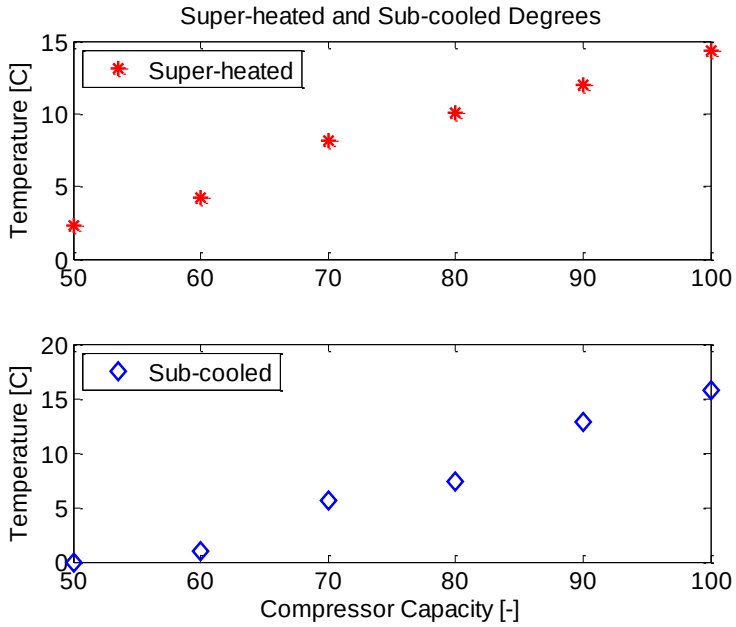

Figure 3.20: Amount of super-heated and sub-cooled degrees added by recuperator

The system has its higher COP at compressor capacity 50% as shown in figure 3.8 but at this point the recuperator add zero sub-cooled degree and only about 2.3 super-heated degree. These amount of super heating is not safe enough to operate the system at this operating point. Hence, selecting the most efficient operating point depends on the cycle and recuperator performance together.

3.4 Shutdown Procedure

The shutdown procedure starts with reducing the compressor capacity. it is preferable to reduce the compressor capacity 10% for each step. When the compressor capacity reaches 10%, shutdown the compressor. Reducing the compressor capacity before shut it down is better to prevent any shock or damage to the compressor valves. After that open the expansion valve to its fully-open position and then shutdown the TCB. If the shutdown data is required and should be recorded, keep the power supplies and DAQs on until the system reaches the initial state again. After that, save the recorded data on the workstation. Each program has different way to save the data. Finally, shutdown the DAQs, power supply and the workstations.

Chapter 4

VCC Modeling and Validation

4.1 Component Modeling

4.1.1 Plate Heat Exchanger

Plate heat exchanger is one of the most efficient heat exchangers due to the design of the corrugated plates and the narrow passage between them. In this thesis two identical plate heat exchangers are used as evaporator and recuperator with the dimensions shown in Figure 4.1

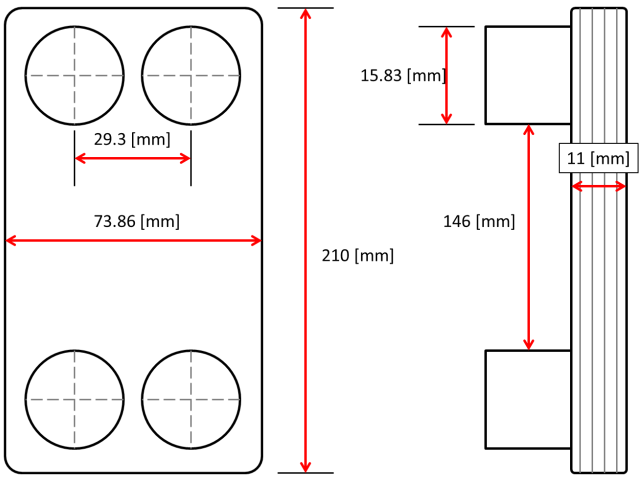

Figure 4.1: Plate heat exchanger dimensions

The distance between the plates is known as the mean channel flow gap and it is equal to 1 mm. The heat exchanger plates are corrugated type. In order to express the increase of the plates length an enlargement factor ϕ is used:

$$\phi = \frac{Developed\ length}{Projected\ length} \tag{4.1}$$

The enlargement factor or (effective plate length) ϕ has standard values based on manufacturer. These values vary between 1.1 and 1.42. The enlargement factor of the plate heat exchanger used in this thesis is 1.4.

The hydraulic diameter of the plate heat exchanger is given as:

$$D_h = \frac{4A_l}{p_w} \tag{4.2}$$

where A_l is the channel flow cross sectional area:

$$A_l = bL_w \tag{4.3}$$

and p_w is the wetted perimeter:

$$p_w = 2\,(b + \phi L_w) \tag{4.4}$$

where L_w is the plate width and b is the mean channel flow gap.

In this section heat transfer models of the evaporator and recuperator are developed. The main goal of this model is to predict the outlet conditions and the length of the different flow zones inside the heat exchangers.

In the evaporator, the refrigerant gains heat from TCB oil. The refrigerant enters and exits the evaporator as a two-phase fluid. Hence, the evaporator has only one flow zone as shown in Figure 4.2

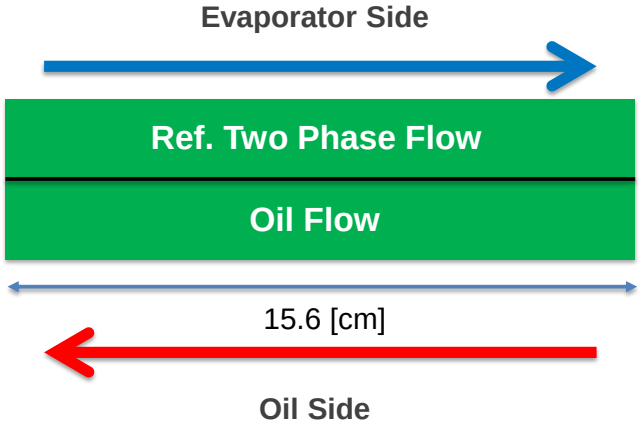

Figure 4.2: Evaporator has single flow zone

In order to model the heat transfer in the evaporator heat balance formulas between refrigerant, plates, and oil should be solved to predict the evaporator outlet condition.

$$\dot{Q}_{evap} = \dot{Q}_{oil} + \dot{Q}_{gain} \tag{4.5}$$

where $\dot{Q}_{gain}$ is the heat gain from the ambient due to natural convection.

The heat transfer of refrigerant side is given as below:

$$\dot{Q}_{evap} = \dot{m}\,(h_o - h_i) \tag{4.6}$$

and

$$\dot{m}\,(h_o - h_i) = \alpha_{evap}\,(T_{sat} - T_w)\,p_w L_P \tag{4.7}$$

where L_P is the plate length between the inlet and outlet ports.

The heat transfer coefficient α_{evap} is given as:

$$\alpha_{evap} = Nu_e \frac{k}{D_h} \tag{4.8}$$

The Nusselt number is calculated based on Kim et al. correlations [31]:

$$Nu_e = 5.323 Re_{eq}^{0.42} Pr_l^{1/3} \tag{4.9}$$

where Re_{eq} is the equivalent Reynolds number [31]:

$$Re_{eq} = \frac{G_{eq} D_h}{\mu_l} \tag{4.10}$$

where G_{eq} is the equivalent mass flux proposed by Akers et al. [4]:

$$G_{eq} = G\left[1 - x_m + x_m \left(\frac{\rho_l}{\rho_v}\right)^{1/2}\right] \tag{4.11}$$

where G is the mass flux and is given by:

$$G = \frac{\dot{m}}{N_{cp} b L_w} \tag{4.12}$$

where N_{cp} is number of channel per passes:

$$N_{cp} = \frac{N_t - 1}{2N_p} \tag{4.13}$$

where N_t and N_p are the total number of plates and the number of passes.

The heat transfer of oil side is given as:

$$\dot{Q}_{oil} = \dot{m}_{oil} C_P \left(T_i - T_o\right) \tag{4.14}$$

and

$$\dot{m}_{oil} C_P \left(T_i - T_o\right) = \alpha_{oil} \left(\bar{T}_{oil} - T_w\right) p_w L_P \tag{4.15}$$

where $\bar{T}_{oil}$ is the averaged oil temperature:

$$\bar{T}_{oil} = \frac{T_i + T_o}{2} \tag{4.16}$$

and α_{oil} is oil heat transfer coefficient given by Equation 4.8, where Nu_{oil} is obtained according to Pradhan et al. formula [50]

$$Nu_{oil} = 0.2 Re_{oil}^{0.75} Pr_{oil}^{0.4} \tag{4.17}$$

and k_{oil} is given by the manufacturer as $0.151\ W/(m.K)$.

The conduction through plates is neglected as an assumption for simplicity. The heat balance between refrigerant and oil flow can be given as:

$$\alpha_e \left(T_w - T_{sat}\right) = \alpha_{oil} \left(\bar{T}_{oil} - T_w\right) \tag{4.18}$$

Equations 4.7, 4.15, and 4.18 have three unknowns and can be solved to predict the specific enthalpy at the evaporator outlet. A nonlinear solver such as fsolve function in Matlab software can be used to solve these equations numerically.

The recuperator transfers the heat from refrigerant at the condenser outlet into refrigerant at the evaporator outlet due to the temperature difference between these two points. In the condenser

side, refrigerant enters the recuperator as a two-phase fluid and exits as a sub-cooled liquid. On the other side, the refrigerant exits the evaporator and enters recuperator as a two-phase fluid and exits as super-heated gas. Since, the scenario of the interaction between these two fluids are unknown, an assumption of dividing the recuperator into three flow zones has been made as shown in Figure 4.3.

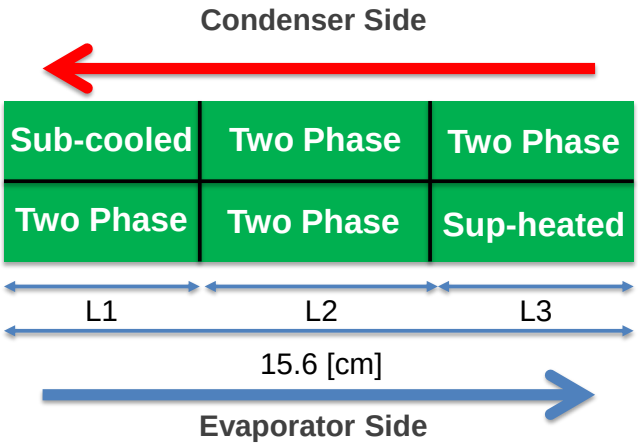

Figure 4.3: Recuperator has three flow zones

The inlet condition of each side is known from the model prediction of both condenser and evaporator. Wall temperature, exit condition and length of each zone are unknowns. In order to predict these values heat balance equations between condenser-refrigerant, heat exchanger wall, and evaporator-refrigerant should be established.

The heat transfer of the first two-phase zone in evaporator side of recuperator is given as:

$$\dot{m}\,(h_{e1} - h_{ei}) = \alpha_{TPe}\,(T_{w1} - T_{sat})\,p_w L_1 \tag{4.19}$$

The two-phase heat transfer coefficient α_{TPe} is given by Equation 4.8 and Nusselt number is calculated by Equation 4.9.

In the second two-phase zone, the same procedure is followed since two-phase flow is still applied with difference in the boundary values:

$$\dot{m}\,(h_{ge} - h_{e1}) = \alpha_{TPe}\,(T_{w2} - T_{sat})\,p_w L_2 \tag{4.20}$$

In the third zone, the fluid becomes super-heated and the heat transfer is given as:

$$\dot{m}\,(h_{eo} - h_{ge}) = \alpha_{ge}\,(T_{w3} - \bar{T}_{ge})\,p_w L_3 \tag{4.21}$$

where $\bar{T}_{ge}$ is the averaged temperature of the super-heated refrigerant.

The heat transfer coefficient of the third zone α_{ge} is given by Equation 4.8. A single phase fluid in thr laminar flow regime has a constant Nusselt number equal to 8.235 [41].

In the condenser side of recuperator, the same procedure is followed with three heat transfer equations for the three zones as below:

$$\dot{m}\,(h_{ci} - h_{c1}) = \alpha_{TPc}\,(T_{sat} - T_{w3})\,p_w L_3 \tag{4.22}$$

$$\dot{m}\,(h_{c1} - h_{fc}) = \alpha_{TPc}\,(T_{sat} - T_{w2})\,p_w L_2 \tag{4.23}$$

$$\dot{m}\,(h_{fc} - h_{co}) = \alpha_{fc}\,(\bar{T}_{fc} - T_{w1})\,p_w L_1 \tag{4.24}$$

where $\bar{T}_{fc}$ is the averaged temperature of the cub-cooled refrigerant.

The two-phase heat transfer coefficient α_{TPc} is calculated based on Shah's formula [53]:

$$\alpha_{TPc} = \alpha_{lo}\left[(1-x)^{0.8} + \frac{3.8x^{0.76}\,(1-x)^{0.04}}{P_{red}^{0.38}}\right] \tag{4.25}$$

where α_{lo} is the liquid only heat transfer coefficient [53]:

$$\alpha_{lo} = 0.023 Re_{lo}^{0.8} Pr_l^{0.4} \frac{k_l}{D} \tag{4.26}$$

and P_{red} is the reduced pressure [53]:

$$P_{red} = \frac{P_{cond}}{P_{crit}} \tag{4.27}$$

The liquid only Reynolds number is given as:

$$Re_{lo} = \frac{GD}{\mu_l} \tag{4.28}$$

The heat transfer coefficient of the sub-cooled zone α_{fc} is given as below:

$$\alpha_{cond} = Nu_c \frac{k}{D_h} \tag{4.29}$$

A single phase fluid in the laminar flow regime has a constant Nusselt number Nu_c equal to 8.235 [41].

The conduction through recuperator plates is neglected as an assumption for simplicity. The heat balance between condenser side refrigerant and evaporator side refrigerant for the three zones are given by equations [4.30-4.32] below:

First zone (Two-phase evaporator and sub-cooled condenser):

$$\alpha_{TPe}\left(T_{w1} - T_{sat}\right) = \alpha_{fc}\left(\bar{T}_{fc} - T_{w1}\right) \tag{4.30}$$

Second zone (Two-phase evaporator and two-phase condenser)::

$$\alpha_{TPe}\left(T_{w2} - T_{sat}\right) = \alpha_{TPc}\left(T_{sat} - T_{w2}\right) \tag{4.31}$$

Third zone (Super-heated evaporator and two-phase condenser):

$$\alpha_{ge}\left(T_{w3} - \bar{T}_{ge}\right) = \alpha_{TPc}\left(T_{sat} - T_{w3}\right) \tag{4.32}$$

Finally, the recuperator length is divided into three zones which must satisfy:

$$L_{cond} = L_1 + L_2 + L_3 \tag{4.33}$$

Equations (4.19-4.24) and Equations(4.30-4.33) have ten unknowns and can be solved to predict the outlet condition of both recuperator sides. Also, the recuperator moving boundary model is able to predict the effect of changing the operating condition on the amount of super-heated and sub-cooled degrees that can be added by using the recuperator. A nonlinear solver such as the Fsolve function in Matlab software can be used to solve these equations numerically.

4.1.2 Fin-Tube Heat Exchanger

In this section a heat transfer models of the air cooled condenser is developed. The main goal of this model is to predict the outlet condition of the condenser and the length of the super-heated and two phase zones. Table 2.2 showed the condenser dimensions and materials.

Heat balances between refrigerant, pipe wall, and air flow across the condenser are handled. The flow inside the condenser is divided into two main regions as shown in Figure 4.4. In the first part, the refrigerant is in the gaseous form since it exits the compressor as super-heated vapor. The second part contains the two phase flow of the refrigerant, where the gas start to condense.

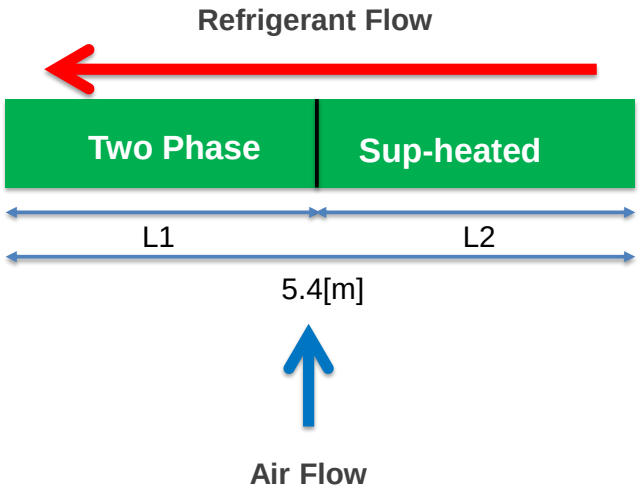

Figure 4.4: Condenser has two flow regions

In order to model and predict the outlet condition of the condenser and the length of each zone, there are five equations to be solved since there are two different flow regimes. The heat transfer in the super-heated part is given as:

$$\dot{m}\,(h_i - h_g) = \alpha_v\,(T_v - T_{w1})\,A_{s1} \tag{4.34}$$

where A_{s1} is the surface area of the first part of condenser:

$$A_{s1} = p_w L_v \tag{4.35}$$

where p_w is the wetted perimeter and L_v is the super-heated zone length.

The fin-tube heat exchanger combines straight pipes, curvatures, and fins in its design. In order

to calculate the heat transfer coefficient, these combinations should be taken into account. The heat transfer coefficient of the vapor region of the condenser is calculated as:

$$\alpha_v = \frac{(\alpha_{vc} A_{sc}) + (\alpha_{vp} A_{sp})}{A_T} \tag{4.36}$$

where

$$\alpha = Nu \frac{k}{D_h} \tag{4.37}$$

where k is the thermal conductivity of the fluid.

The effect of the curvatures and straight pipes combinations are weighted based on their surface areas into the total surface area of the condenser. The Nusselt number of curvature pipe is calculated based on Acharya et al. correlations [2]:

$$Nu_c = 0.69 \delta^{0.13} Re^{0.5} Pr^{0.43} \quad for \ Pr \leq 1 \tag{4.38}$$

$$Nu_c = 0.67 \delta^{0.13} Re^{0.5} Pr^{0.21} \quad for \ Pr > 1 \tag{4.39}$$

where δ is the radius ratio between the pipe inlet radius and the curvature radius.

For the straight pipe portion of vapor side of the condenser, Nusslet number is calculated based on Gneilinski's formula [26]:

$$Nu_p = \frac{(f/8)(Re - 1000) Pr}{1 + 12.7 (f/8)^{(1/2)} \left(Pr^{2/3} - 1\right)} \tag{4.40}$$

where f is given based on Petukhov's formula [49]:

$$f = (0.79 ln(Re) - 1.64)^{-2} \tag{4.41}$$

For the two phase flow region, the heat transfer is given as:

$$\dot{m} (h_g - h_o) = \alpha_{TP} (T_{TP} - T_{w2}) A_{s2} \tag{4.42}$$

where A_{s2} is the surface area of the two-phase zone of the condenser:

$$A_{s2} = p_w L_{TP} \tag{4.43}$$

L_{TP} is the length of the two phase zone of the condenser.

For heat transfer coefficient calculation, same procedure is followed:

$$\alpha_{TP} = \frac{(\alpha_{TPc} A_{sc}) + (\alpha_{TPp} A_{sp})}{A_T} \tag{4.44}$$

Heat transfer coefficient for the straight pipe portion is calculated based on Shah's formula [53]:

$$\alpha_{TPp} = \alpha_{lo} \left[(1-x)^{0.8} + \frac{3.8 x^{0.76} (1-x)^{0.04}}{P_{red}^{0.38}} \right] \tag{4.45}$$

where α_{lo} is the liquid only heat transfer coefficient [53]:

$$\alpha_{lo} = 0.023 Re_{lo}^{0.8} Pr_l^{0.4} \frac{k_l}{D} \tag{4.46}$$

and P_{red} is the reduced pressure [53]:

$$P_{red} = \frac{P_{cond}}{P_{crit}} \tag{4.47}$$

The liquid only Reynolds number is given as:

$$Re_{lo} = \frac{GD}{\mu_l} \tag{4.48}$$

The heat transfer coefficient for the curved pipe α_{TPc} is calculated by Equation 4.37, where Nusslet number is given based on Naphon and Wongwises correlation [44]:

$$Nu_{TPc} = 2.3 (Re^*)^{0.94} Pr^{0.4} \tag{4.49}$$

where

$$Re^* = \frac{GxD_i}{\mu_l \sqrt{\rho_l / \rho_v}} \tag{4.50}$$

After that a heat balance equation between refrigerant and external air flow is calculated. The same procedure of separating the condenser into super-heated and two-phase region is followed.

$$\alpha_v (T_v - T_{w1}) p_w L_v = \alpha_{air} (T_{w1} - T_{amb}) A_{sT1} \tag{4.51}$$

where A_{sT1} is the total surface area of the pipe and fins for vapor region.

For the two-phase region, the heat balance equation is written as:

$$\alpha_{TP}\left(T_{TP}-T_{w2}\right)p_w L_{TP}=\alpha_{air}\left(T_{w2}-T_{amb}\right)A_{sT2} \tag{4.52}$$

where A_{sT2} is the total surface area of the pipe and fins for two-phase zone.

The total air heat transfer coefficient is a combination of two different heat transfer coefficients. The first one is a heat transfer coefficient between two plates (fins), while the other one is a heat transfer coefficient around a cylinder. These two coefficients are weighted based on their surface areas contribution:

$$\alpha_{air}=\frac{\left(\alpha_{air_f}A_{sf}\right)+\left(\alpha_{air_p}A_{sp}\right)}{A_{air_T}} \tag{4.53}$$

The heat transfer coefficient is calculated by Equation 4.37, where Nusslet number across a cylinder is given as suggested by Churchill and Bernstein [21]:

$$Nu=0.3+\frac{0.62Re^{1/2}Pr^{1/3}}{\left[1+(0.4/Pr)^{2/3}\right]^{1/4}};\quad Re<10^4 \tag{4.54}$$

$$Nu=0.3+\frac{0.62Re^{1/2}Pr^{1/3}}{\left[1+(0.4/Pr)^{2/3}\right]^{1/4}}\left[1+\left(\frac{Re}{282,000}\right)^{1/2}\right];\quad 2\times10^4<Re<4\times10^5 \tag{4.55}$$

$$Nu=0.3+\frac{0.62Re^{1/2}Pr^{1/3}}{\left[1+(0.4/Pr)^{2/3}\right]^{1/4}}\left[1+\left(\frac{Re}{282,000}\right)^{5/8}\right]^{4/5};\quad 4\times10^5<Re<5\times10^6 \tag{4.56}$$

For the laminar flow between two plates, Nusslet number is constant and it equals to 8.235 [41].

The condenser total length constraint is:

$$L_{cond}=L_v+L_{TP} \tag{4.57}$$

Equations 4.34, 4.42, 4.51, 4.52, and 4.57 have five unknowns and can be solved to predict the specific enthalpy at the condenser outlet and the length of the super-heated and two-phase zones of the condenser. A nonlinear solver such as the Fsolve function in Matlab software can be used to solve these equations numerically.

4.1.3 Linear Compressor

The compressor used in this work is a piston-cylinder compressor type that uses a linear motor to drive the piston. Compressor capacity is controllable and can be changed from 1% to 100%. When the compressor capacity changes the piston stroke length changes which means changing in the compression volume. However, the compressor frequency is constant for the whole range of the compressor capacity and equal to 332.6 s^{-1}. Since the compression volume changes with changing the compressor capacity, the volumetric efficiency will also change. Volumetric efficiency is a function of the pressure ratio across the compressor:

$$\eta_v = a\left(\frac{P_{out}}{P_{in}}\right)^b + c \tag{4.58}$$

where a,b and c are constants obtained from experimental data.

The outlet pressure is calculated then as per Liang et al. forumla [38]:

$$P_{out} = P_{in}\left[\frac{(1-\eta_v)}{CR} + 1\right]^k \tag{4.59}$$

where CR is the geometric compression ratio and k is the specific heat ratio.

The outlet specific enthalpy is calculated based on:

$$h_{out} = h_{in} + \frac{(h_{outS} - h_{in})}{\eta_S} \tag{4.60}$$

where h_{outS} is the outlet specific enthalpy under isentropic process and η_S is the isentropic efficiency:

$$\eta_S = d\left(\frac{P_{out}}{P_{in}}\right)^e + f \tag{4.61}$$

where d,e and f are constants obtained from experimental data.

By solving Equations 4.59 and 4.60 the compressor outlet condition is obtained.

4.1.4 Expansion Valve

The main role of throttling device is to control refrigerant flow by changing the cross sectional area. The throttling device that used in this work is a metering valve from Swagelok Company with dimensions mentioned in Figure 4.5

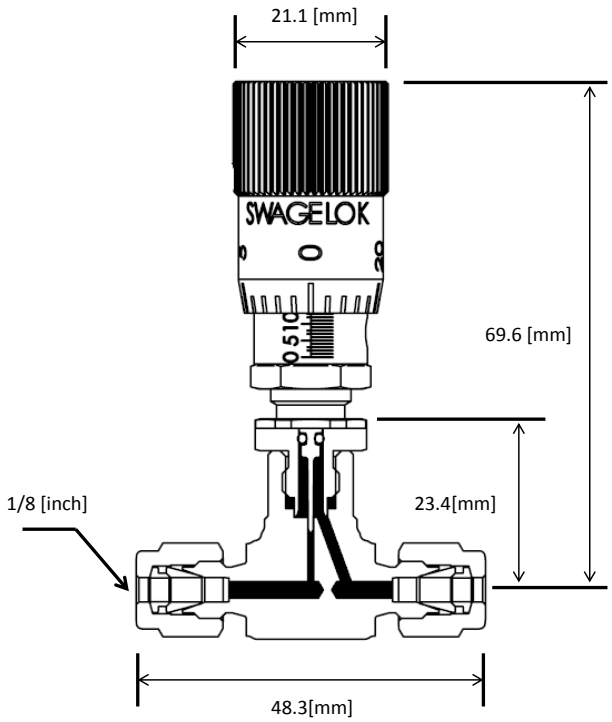

Figure 4.5: Swagelok metering valve dimensions

Mass flow rate across the expansion valve is governed as below:

$$\dot{m} = C_v \sqrt{\rho_{in} \left(P_{in} - P_{out} \right)} \tag{4.62}$$

where C_v is the flow coefficient of the valve.

The C_v value is a function of the cross sectional area, the fluid specifications and pressure difference. It is not easy to specify this value, so an empirical value is giving to this parameter based on experiments as below:

$$C_v = aA_V + bA_V^2 + c\left(\frac{P_{in}}{P_{out}}\right) \tag{4.63}$$

where a,b and c are constants obtained from experimental data.

4.1.5 Heat Loss/gain

The heat loss/gain in the evaporator, recuperator and VCC copper pipes are estimated as bare component (without any insulation) to predict the maximum heat loss/gain. For the evaporator and recuperator a natural flow on a vertical wall is used to calculate the heat gain from the ambient.

$$\dot{Q}_{g_{HX}} = \alpha_{nc} A_s \left(T_{amb} - T_w\right) \tag{4.64}$$

The wall temperature is predicted by using the plate heat exchanger model mentioned in Section 4.1.1. The natural convection heat transfer coefficient is given by:

$$\alpha_{nc} = Nu_{nc} \frac{k_{air}}{D_h} \tag{4.65}$$

where Nusselt number is calculated based on Churchill and Chu correlations [22]:

$$Nu_{nc} = 0.68 + 0.67 \left(Ra_L \Psi\right)^{1/4}; \quad Ra_L < 10^9 \tag{4.66}$$

$$Nu_{nc} = 0.68 + 0.67 \left(Ra_L \Psi\right)^{1/4} \left(1 + 1.6 \times 10^{-8} Ra_L \Psi\right)^{1/12}; \quad 10^9 < Ra_L 10^9 < 10^{12} \tag{4.67}$$

where Ra_L is Rayleigh number defined as:

$$Ra_L = Gr_x Pr \tag{4.68}$$

Gr_x is the Grashof number given by:

$$Gr_x = \beta \Delta T g x^3 / \nu^2 \tag{4.69}$$

where

$$\beta = \frac{1}{T_{amb}} \tag{4.70}$$

The Prandtl number function Ψ is defined as [41]:

$$\Psi = \left[1 + \left(\frac{0.492}{Pr}\right)^{9/16}\right]^{-16/9} \tag{4.71}$$

Note: Equations 4.66 and 4.67 do not match exactly at $Ra_L \sim 10^9$ [41].

For the cycle pipes, the heat loss/gain is calculated as a natural flow on a horizontal cylinder (Most of the cycle pipe connections are in a horizontal orientation). The heat transfer per meter length is given as:

$$\dot{Q}_{gPipe} = \alpha_{nc} \pi D_h \left(T_{amb} - T_w\right) \tag{4.72}$$

The heat transfer coefficient is given by Equation 4.65 where Nusslet number is given by Churchill and Chu correlations[22]:

$$Nu_{nc} = 0.36 + \frac{0.518 Ra_D^{1/4}}{\left[1 + \left(\frac{0.559}{Pr}\right)^{9/16}\right]^{4/9}}; \quad 10^{-6} < Ra_L < 10^9 \tag{4.73}$$

$$Nu_{nc} = \left(0.6 + 0.387 \left[\frac{Ra_D}{\left[1 + \left(\frac{0.559}{Pr}\right)^{9/16}\right]^{16/9}}\right]^{1/6}\right)^2; \quad Ra_L > 10^9 \tag{4.74}$$

The heat loss/gain prediction from Equations 4.64 and 4.72 are used back in Equation 4.6.

4.2 Cycle Modeling

In order to predict the vapor compression cycle behavior as a whole unit under changing operation conditions a cycle model is presented in this section. The cycle model should be self sufficient and depends only on external boundary conditions. Air velocity and ambient temperature at the condenser side and oil mass flow rate and inlet temperature at the evaporator side are the only boundary condition inputs into the cycle model. Component models mentioned in the previous section (Section 4.1) are combined and integrated together in one model to predict the cycle model.

Cycle model contains 22 equations with 22 unknowns integrated from the component sub-model as mentioned in Table 4.1. In addition, the model can predict the averaged wall temperatures of condenser, evaporator, and recuperator at different zones. The Fsolve function in Matlab software has been used to solve these equations.

Cycle Level	
Mass Flow Rate	[kg/s]
Compressor	
Outlet Pressure	[kPa]
Outlet Specific Enthalpy	[J/kg]
Condenser	
Vapor Zone Length	[m]
Two-phase Zone Length	[m]
Outlet Specific Enthalpy	[J/kg]
Expansion Valve	
Outlet Pressure	[kPa]
Evaporator	
Outlet Specific Enthalpy	[J/kg]
Oil Exit Temperature	[K]
Recuperator	
Evaporator Side Outlet Specific Enthalpy	[J/kg]
Condenser Side Outlet Specific Enthalpy	[J/kg]
Two-phase/Sub-cooled segment Length	[m]
Two-phase/Two-phase segment Length	[m]
Super-heated/Sub-cooled segment Length	[m]

Table 4.1: Main data that cycle model can predicts

The next section discusses the validation of the all models mentioned in this section and show the agreement between the model prediction and the experimental results.

4.3 Component Model Validation

In the previous section (section 4.1), detailed component models have been discussed to predict the component behaviors under changing operation conditions. In this section, model validation is handled to show how well the models agree with the experimental data.

All component models have been validated with experimental data to predict inlet and outlet conditions of each component. Figure 4.6 shows the P-h diagram for the VCC test bed at different operating points (different compressor capacities). The graph shows a very good agreement between the experimental data and component model predictions. Additionally, evaporator, condenser and recuperator models have other results that will be mentioned in details in the following parts.

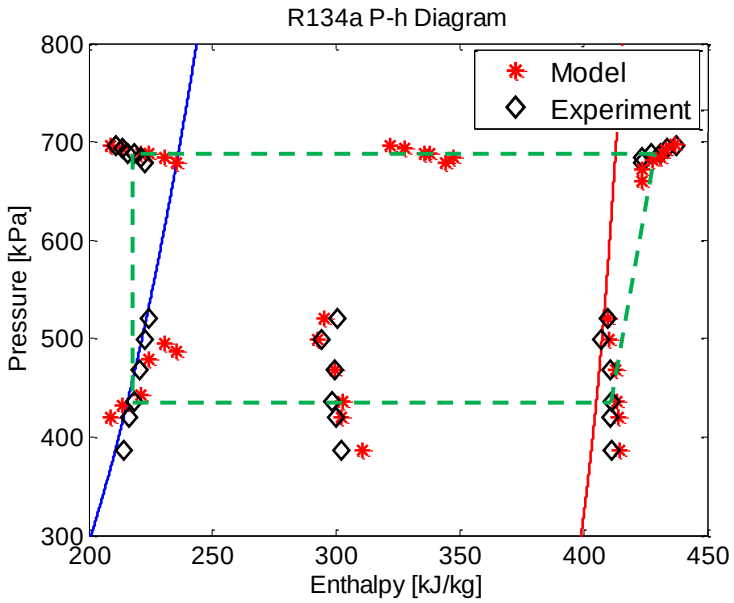

Figure 4.6: Components model validation

4.3.1 Evaporator

The main goal of the evaporator model is to predict the refrigerant status at the evaporator exit as shown in Figure 4.6. Additionally, the model aims to predict the oil outlet temperature. Figure 4.7 shows oil outlet temperature at different compressor capacities.

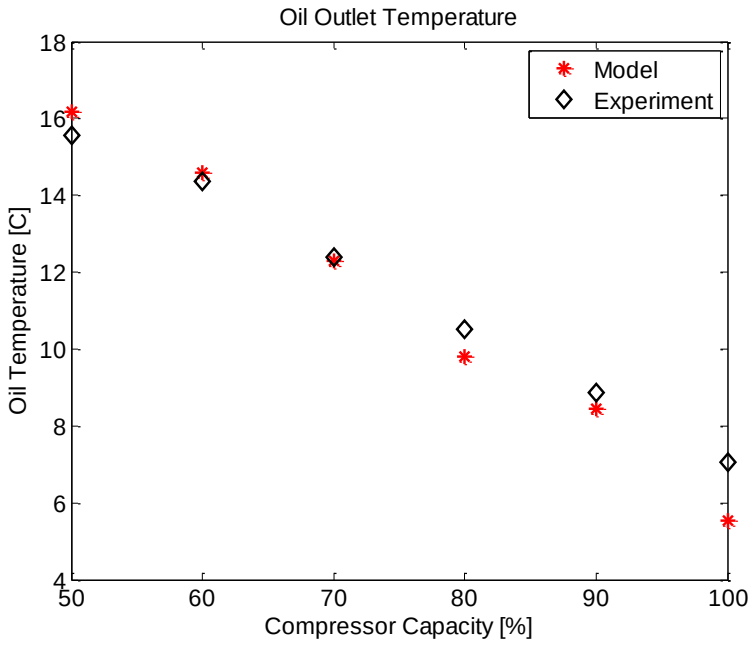

Figure 4.7: Oil outlet temperature

The model result shows a good agreement with experimental data. The temperature measure-

ment uncertainty is around 1.7% of 1 of 1 °C.

4.3.2 Condenser

The condenser model is able to predict the length of super-heated and two-phase lengths in the condenser. At different operation condition these two lengths change as shown in Table 4.2.

Compressor Capacity [%]	Vapor Length [m]	Two-phase Length [m]
50	1.7103	3.6897
60	1.7662	3.6338
70	1.8565	3.5435
80	1.9996	3.4004
90	2.0352	3.3648
100	2.0806	3.3194

Table 4.2: Condenser sub-lengths

As the compressor capacity increases the amount of heat added to the refrigerant is also increases which means more super-heated degree. As a result, refrigerant will need more time (pipe length) to reach the saturation vapor point. Hence, two-phase length reduces with increasing the compressor capacity.

This decrease has a direct effect on recuperator heat load. The refrigerant will enter the recuperator at higher quality as a result of decreasing the two-phase length of the condenser. Since the condenser side of the recuperator is coupled with the evaporator side, the heat load of recuperator increases with decreasing the two-phase length of the condenser as shown in Figure 4.8.

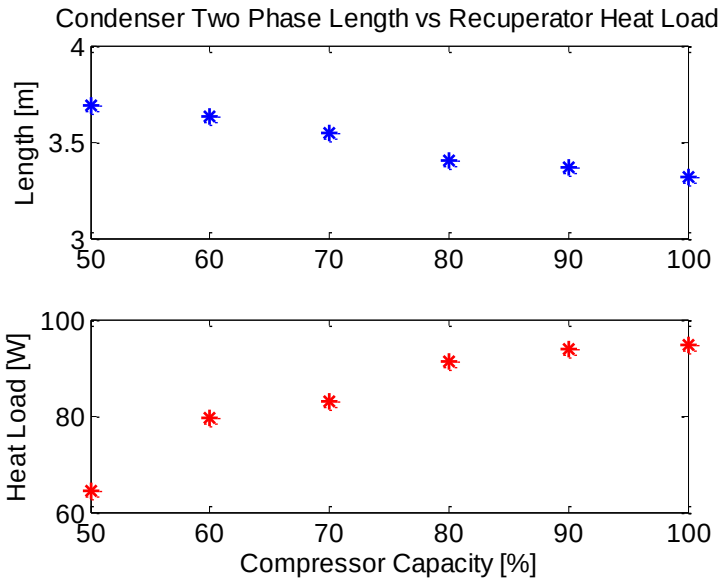

Figure 4.8: Recuperator load vs two-phase zone length

4.3.3 Recuperator

The recuperator model is able to predict the different zone lengths inside the recuperator as mentioned in Section 4.1.1. Knowning the length of super-heat at evaporator side and sub-cooled at condenser side of the recuperator will help to predict the most efficient operation point as discussed in Section 3.3. Figure 4.9 shows the effect of changing the compressor capacity on different zones lengths of recuperator.

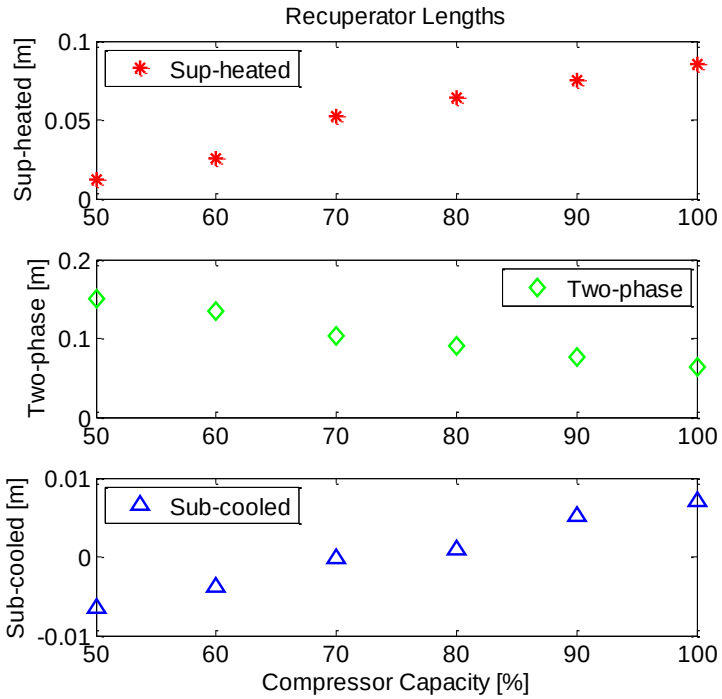

Figure 4.9: Recuperator different zones length

At compressor capacity [50%] the length of sub-cooled is equals to zero while the length of the super-heat zone is less then 0.02 [m]. These values agree with the amount of super-heat and sub-cooled added to the refrigerant as shown in Figure 3.20.

4.4 Cycle Model Validation

The cycle model has been discussed in Section 4.2. The model is self sufficient and needs only two boundary conditions to predict the loop behavior under changing operation conditions. Figures 4.10, 4.11, and 4.12 show the cycle model validation at three different operating points. They show very good agreement between cycle model and experimental data.

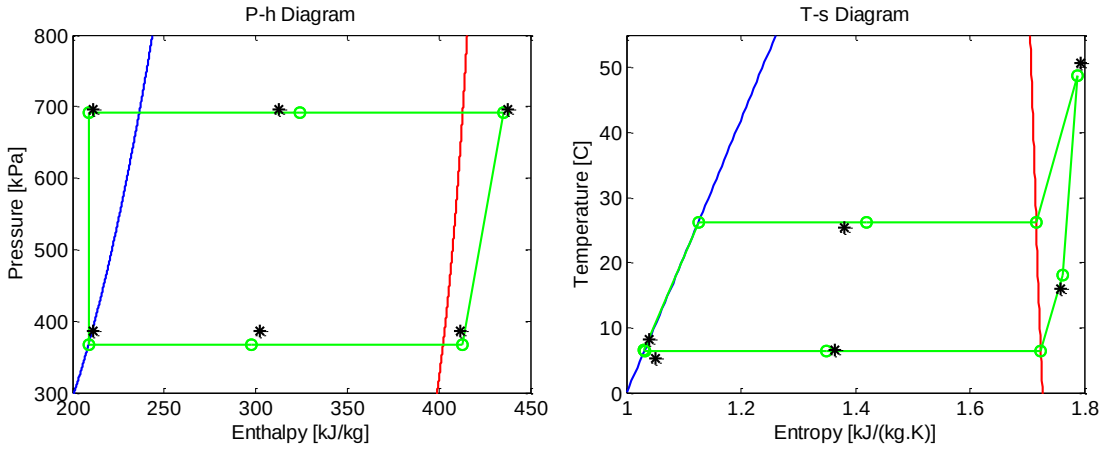

Figure 4.10: Cycle Model at Compressor Capacity 100%

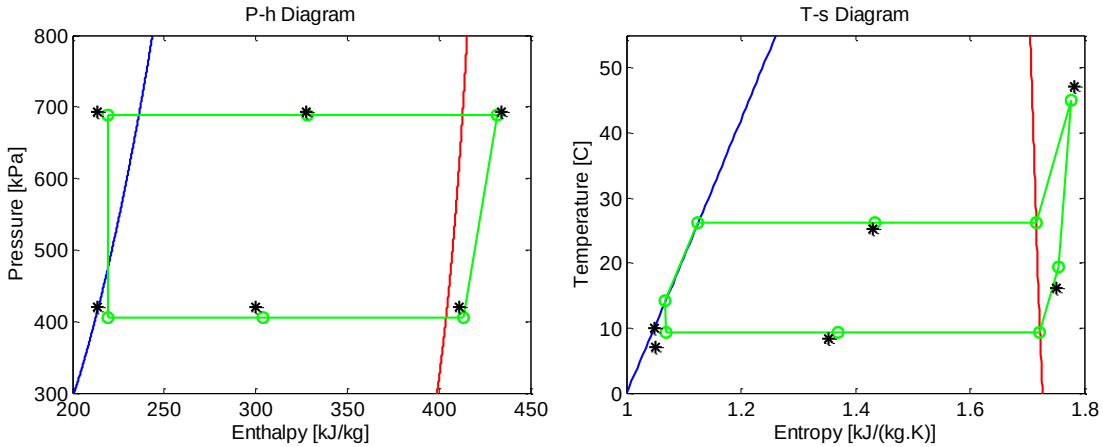

Figure 4.11: Cycle Model at Compressor Capacity 90%

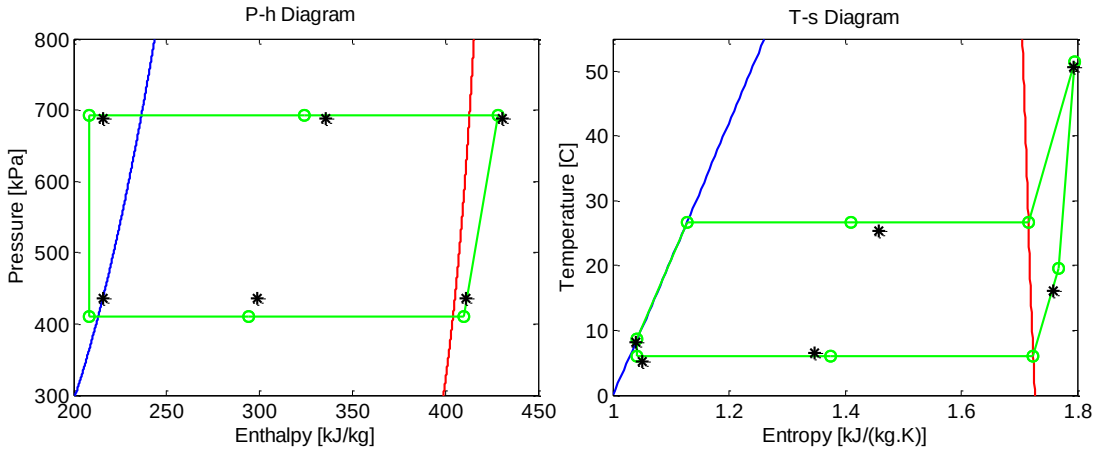

Figure 4.12: Cycle Model at Compressor Capacity 80%

Figure 4.13 shows mass flow rate validation with experimental results. Mass flow meter cali-

bration data are mentioned in Chapter 2.

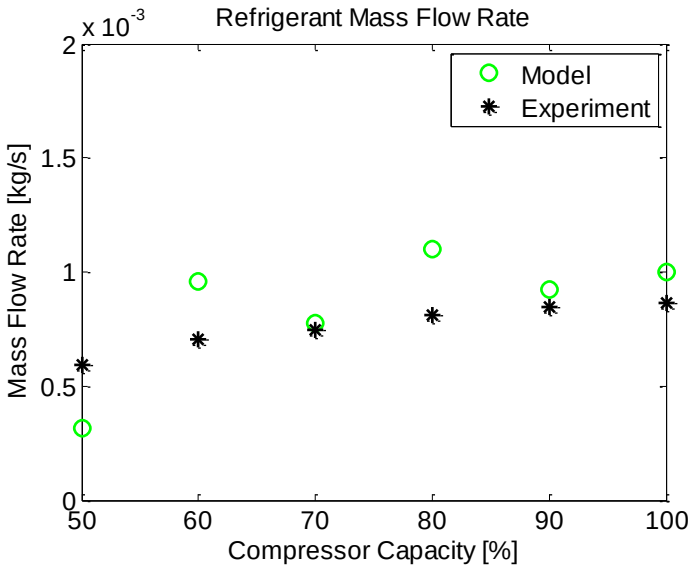

Figure 4.13: Refrigerant mass flow rate at different compressor capacities

The cycle model introduced in this thesis is able to predict the cycle behavior under changing the cycle configuration, changing the components sizes or even using different working fluid. Following are some ideas about using the proposed cycle model for different cases:

1. Install recuperator between compressor inlet and exit to utilize the heat from the hot refrigerant at the exit of the compressor to heat up the refrigerant at the compressor inlet.

2. The effect of changing the recuperator size and capacity on the other components performance.

3. The effect of using different gases such as hydrocarbons as working fluid instead of R134a that was used in this analysis on the components performance and overall performance of the cycle.

Chapter 5

Conclusion and Future Work

A VCC prototype was developed with step-by-step guideline of test-bed configuration, material selection, and construction including safe procedure for components assembly, leakage test, insulation and refrigerant charging (Chapter 2). In Chapter 3, comprehensive and detailed guidelines were given for safe cycle start-up, operation and shut down. A compact VCC prototype was designed and developed, with R134a chosen as a working fluid. Extensive parametric studies were carried out with results discussion to better understand system characteristics and behavior under changing operating conditions. Detailed component and cycle level modeling of the VCC test-bed was developed. As for Chapter 4, moving boundary modeling for recuperator and condenser was handled to find out the effect of changing the operating condition on these heat exchangers performance. The proposed components and cycle models were validated with experimental results. Components and cycle models show very good agreements with experimental results.

Using recuperator-based vapor compression cycle showed better performance with COP around 4.5 at compressor capacity 50% and expansion valve opening position 4. At this operation point, the recuperator was able to transfer around 65 W between condenser exit and evaporator exit. Moving boundary model of recuperator was able to predict the amount of super-heat and sub-cooled degrees that recuperator can add to the refrigerant at different operating points. The model is coupled with other component models and integrated into a cycle-level model. This developed model has very good potential to be used as a design tool for cycle optimization, cycle configuration, and components scaling. On the other hand, the VCC test-bed could be used as a solid foundation for further research topics using different working fluids, different

components scale and various cycle configurations.

Further investigations are desirable. Pressure drop component and cycle level models can be developed. Transient modeling to study the cycle response on changing one component operating point is another possible area of research. The prototype itself can be upgraded by installing different compressor types such as scroll compressor or developing different configurations by using the recuperator between compressor inlet and outlet. Using hydrocarbon gases as working fluids is one of the highly possible area of development for this work. HC gases have have zero ODP and negligible GWP and considered as a strong alternative to replace HFCs. They have similar thermo-physical properties with commonly used refrigerants.

This study contributes to the development of energy-efficient recuperator-based compact vapor compression cycle. It shows the needs of such systems for compact and portable cooling applications. While this work needs more investigation and in-depth understanding at component and cycle level, the technical information presented in this work shows the potential of the compact VCC systems as a solution for electronic and portable cooling applications.

Appendix A

Appendix: Linear Compressor Modeling

Alzoubi et al. [6] performed a theoritical analysis and a parametric study of the transient pressure and temperature profiles inside the compression chamber. They discussed the effect of changing piston velocity on the pressure and temperature trends.

A.1 Theoretical Analysis

A linear micro-compressor consists primarily of two chambers (control volumes). The compression process of the working fluid takes place in the main chamber; while the second chamber contains the linear motor, springs and other parts as shown in Figure A.1. In order to characterize the transient changes of temperature and pressure inside each control volume, mass and energy governing equations are used.

A.1.1 Governing Principles

The main objective of this modeling work is to predict the mass, temperature and pressure changes inside the compressor chambers. In this research, the two independent thermodynamic variables are density and internal energy, while the conjugate variables are temperature and pressure.

$$T = T(\rho, u) \tag{A.1}$$

$$P = P(\rho, u) \tag{A.2}$$

This analysis will employ the mass and energy conservation equations for each chamber to predict the transient changes of density and specific internal energy. Based on the relations in Eq. A.1 and A.2, temperature and pressure profiles can be predicted. The working fluids in this study are assumed to be superheated over the entire compression cycle [14]. The general form of mass balance equation can be written as below:

$$\frac{dm_1}{dt} = \dot{m}_{in} - \dot{m}_{out} \tag{A.3}$$

As shown in Figure A.1, there are two regions where refrigerant can either enter or exit the compression chamber.

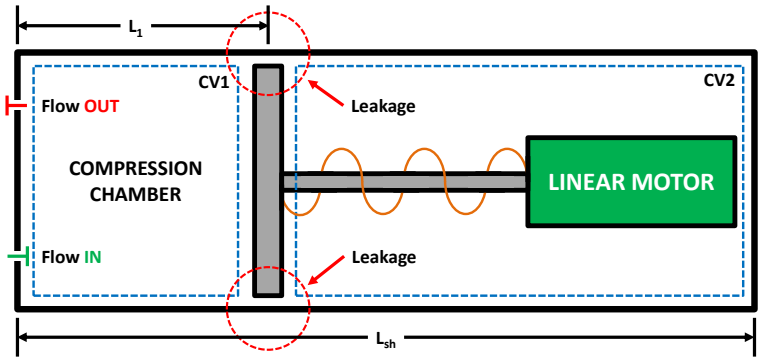

Figure A.1: Schematic diagram of the linear-compressor

The primary flows are the flows through the suction and discharge valves, while the secondary flow is the leakage through the gap between the piston and the compression chamber wall. Also, mass flow rate change can be considered as density and volume rate change. By considering all of the above, Eq. A.3 can be written as follows:

$$\frac{d\rho_1}{dt} = \frac{1}{A_1 L_1}\left[\dot{m}_{1\_in} - \dot{m}_{1\_out} - \rho_1 A_1 U_P\right] \tag{A.4}$$

where:

$$\dot{m}_{1\_in} = \dot{m}_{valve\_in} + \dot{m}_{1\_leak\_in} \tag{A.5}$$

and

$$\dot{m}_{1\_out} = \dot{m}_{valve\_out} + \dot{m}_{1\_leak\_out} \tag{A.6}$$

Eq. A.4 represents the density change in the compression chamber. The change in the second

chamber is almost the same except the fluid is flowing through the leakage area only:

$$\frac{d\rho_2}{dt} = \frac{1}{(A_{sh}L_{sh}) - (A_1L_1)} \left[\dot{m}_{2\_in} - \dot{m}_{2\_out} - \rho_2 A_1 U_P\right] \tag{A.7}$$

where:

$$\dot{m}_{2\_in} = \dot{m}_{2\_leak\_in} \tag{A.8}$$

and

$$\dot{m}_{2\_out} = \dot{m}_{2\_leak\_out} \tag{A.9}$$

The conservation of energy equation can be written in the general form:

$$\frac{dE}{dt} = \dot{Q} + \dot{W} + \sum \dot{m}_{in} h_{in} - \sum \dot{m}_{out} h_{out} \tag{A.10}$$

Assuming that the fluid inside each chamber is well mixed [14], specific enthalpy h_{out} becomes h_1 for the compression chamber and h_2 for the second chamber. Also, the net kinetic and potential energies are small enough to be neglected for both control volumes [43]. The energy rate change can be expressed as the changes in mass and internal energy. The energy rate change for the compression chamber can be written as:

$$\frac{dE_1}{dt} = \frac{d\,(mu)_1}{dt} = m_1 \frac{du_1}{dt} + u_1 \frac{dm_1}{dt} \tag{A.11}$$

In both chambers, the work is done on the system as boundary work. In the compression process, the motor pushes the piston to compress the fluid. Meanwhile, the spring is expanding and storing potential energy. This energy will pull the piston back during the intake stroke, allowing the fluid to enter the compression chamber. While the piston is compressing the fluid in CV1, the other control volume CV2 is expanding at the same time. The work done on the compression chamber is expressed as below:

$$\dot{W}_1 = P_1 \frac{dV_1}{dt} = P_1 A_1 U_P \tag{A.12}$$

By combining Eq. A.11 and A.12, Eq. A.10 becomes:

$$\frac{du_1}{dt} = \frac{1}{\rho_1 A_1 L_1}\left[\dot{Q}_1 + P_1 A_1 U_P + \dot{m}_{valve\_in}\left(h_{valve\_in} - u_1\right) + \right.$$
$$\left. \dot{m}_{1\_leak\_in}\left(h_2 - u_1\right) - \dot{m}_{valve\_out}\left(\frac{P_1}{\rho_1}\right) - \dot{m}_{1\_leak\_out}\left(\frac{P_1}{\rho_1}\right)\right] \quad \text{(A.13)}$$

The total volume of the compressor is constant; any change in the first control volume will equal the change in the second control volume.

$$\frac{dV_2}{dt} = \frac{d\left(V_T - V_1\right)}{dt} = \frac{\cancelto{0}{dV_T}}{dt} - \frac{dV_1}{dt} = -\frac{dV_1}{dt} \quad \text{(A.14)}$$

Based on Eq. A.14 the boundary work acting on CV2 is expressed as below:

$$\dot{W}_2 = P_2 \frac{dV_2}{dt} = -P_2 A_1 U_P \quad \text{(A.15)}$$

The energy balance for the second chamber CV2 then becomes:

$$\frac{du_2}{dt} = \frac{1}{\rho_2\left(A_{sh}L_{sh} - A_1 L_1\right)}\left[\dot{Q}_2 - P_2 A_1 U_P \right.$$
$$\left. + \dot{m}_{2\_leak\_in}\left(h_1 - u_2\right) - \dot{m}_{2\_leak\_out}\left(\frac{P_2}{\rho_2}\right)\right] \quad \text{(A.16)}$$

From equations A.4, A.7, A.14 and A.15, both chamber densities and internal energies can be calculated and then the temperature and pressure profiles can be predicted throughout the entire cycle.

A.1.2 Piston Position and Motion Model

Piston motion makes the density and internal energy change inside the compressor. It also causes the leakage between the piston and the compression chamber wall. The piston is powered by a linear motor that has a sinusoidal force. The motion profile for this model is assumed to be the same as the motion profile of a crank-driven piston [11]. The profile that governs the piston motion is given below:

$$U_P = U_{max} \sin\left(\frac{\pi}{t_s} t + \pi\right) \quad \text{(A.17)}$$

Based on Eq. A.17, the piston position through the whole cycle can be predicted.

$$L_1 = L_{min} + U_{max}\left(\frac{t_s}{\pi}\right)\left[1 - \cos\left(\frac{\pi}{t_s}t + \pi\right)\right] \tag{A.18}$$

The time needed to complete one stroke is given as below:

$$t_s = \frac{(L_{max} - L_{min})}{U_{max}}\frac{\pi}{2} \tag{A.19}$$

A.1.3 Valve Model

Refrigerant flow rates through the intake and discharge valves are driven by pressure differences across the valves. The valve can be modeled as a plate valve [32] or as a reed valve [14]. In both cases, the valve can be modeled as an ideal nozzle [54]. The flow through this valve is assumed to be isentropic steady-state flow. From Bernoulli and continuity equations the volumetric flow rate for an incompressible flow is computed as follows:

$$G = A_{low}\sqrt{\frac{1}{1 - \left(\frac{d_{low}}{d_{high}}\right)^4}}\sqrt{2\frac{(P_{high} - P_{low})}{\rho}} \tag{A.20}$$

Where d_{low} and d_{high} are the diameters at the low and high pressure regions respectively. By introducing the diameter ratio, the coefficient of discharge and the expansion factor, the mass flow rate through the valve is:

$$\dot{m}_{valve} = A_{low}\sqrt{2\rho_{high}P_{high}}\sqrt{\frac{\gamma}{\gamma - 1}\left[\left(\frac{P_{low}}{P_{high}}\right)^{\frac{2}{\gamma}} - \left(\frac{P_{low}}{P_{high}}\right)^{\frac{\gamma+1}{\gamma}}\right]} \tag{A.21}$$

When the pressure inside the compression chamber is less than the inlet pressure, the pressure difference will allow the refrigerant to flow through the suction valve. During the compression stroke, the piston compresses the fluid and then increases the pressure. When the pressure inside the chamber becomes larger than the outside pressure, the refrigerant will push the discharge valve and allow the refrigerant to flow out.

A.1.4 Leakage Model

The main leakage occurs between the piston and the compression chamber wall. The pressure difference and the piston movement drive the fluid to flow between the chambers through this

gap. As depicted in Figure A.2, the leakage length is much larger than the gap between the piston and the chamber wall. Therefore, the leakage flow is modeled as a flow between parallel plates.

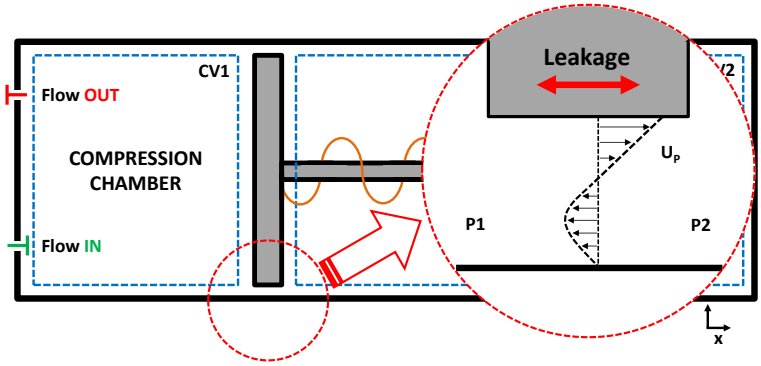

Figure A.2: Leakage flow through the gap between the chamber wall and the piston

The governing equation for this leakage can be modeled using the plane Couette and Poiseuille flow equation [35]

$$\dot{m}_{leak} = \rho_2 A_{leak} \left[\frac{U_P}{2} - \frac{(L_{leak})^2}{12\mu_2} \frac{dP}{dx} \right] \tag{A.22}$$

where

$$\frac{dP}{dx} > 0 \tag{A.23}$$

A.2 Model Prediction

By solving four ordinary differential equations A.4, A.7, A.13, and A.16, the above model can predict the temperature and pressure profile inside the compressor.

In this simulation study, the working fluid is R134a, and the inlet and outlet boundary conditions of the linear micro-compressor are chosen as T_{in}= 5 $^{\circ}C$, P_{in} = 240 kPa and T_{out} = 50 $^{\circ}C$, P_{out} = 500 kPa respectively. Table A.1 lists the main geometric parameters used for the linear compressor in this study.

Parameters	Values
Top Dead Center (TDC) [cm]	0.1
Bottom Dead Center (BDC) [cm]	5
Valve Diameter [cm]	0.3
Leakage Gap [cm]	0.01
Piston Thickness [cm]	3.5
Piston Diameter [cm]	10

Table A.1: Micro-compressor Geometric Parameters

A.2.1 Pressure Profile

To complete the compression cycle, the piston goes through a forward (compression) stroke and backward (suction) stroke. In the compression stroke, the piston compresses the gas inside the compression chamber. While in the suction stroke, the springs pull back the piston and then the fluid enters the chamber due to the pressure difference.

In the compression stroke, and while the fluid is compressed, the pressure and temperature inside the compression chamber increase. When the fluid reaches a pressure equal to or larger than the outlet pressure, the discharge valve opens and allows the fluid to flow out. Consequently, the pressure inside the chamber decreases gradually. The flow continues until the pressure once again becomes lower than the outlet pressure, but still higher than the inlet pressure. The piston stops when it reaches the minimum stroke length.

In the suction stroke, the spring pulls back the piston which allows the fluid to expand and decrease its pressure. The intake valve will not open until the pressure inside the compression chamber becomes less than the inlet pressure. At this point, the suction valve opens and the gas enters the chamber. The spring continues pulling the piston until it reaches the maximum stroke length. The spring pulling force decreases the pressure in the chamber while the inlet flow increases it. Because of these conflicting forces the overall pressure in the chamber rises up slowly until it reaches its initial value. Figure A.3 shows the pressure profile inside the compression chamber through the compression and suction strokes.

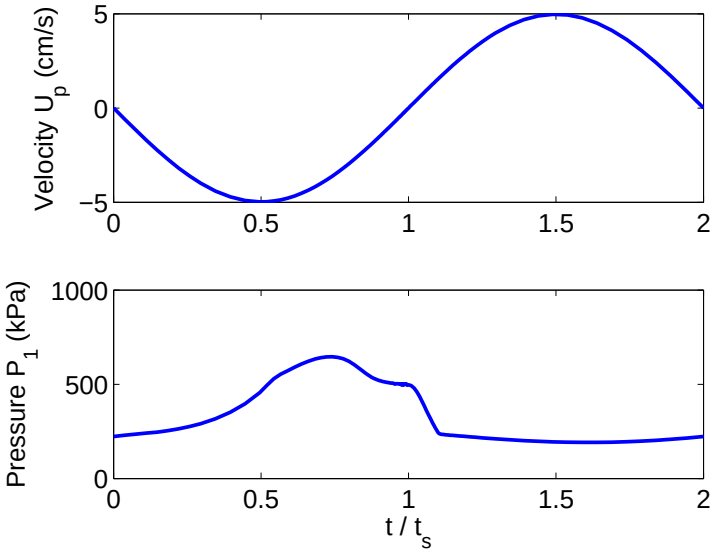

Figure A.3: Pressure profile in the compression chamber

A.2.2 Temperature Profile

Figure A.4 shows the temperature profile inside the compression chamber during the compression process. At the beginning of the compression stroke, the discharge valve stays closed till the pressure inside the chamber becomes higher than the outlet pressure. While the valve is closed, the piston compresses the fluid causing the temperature to rise in the chamber.

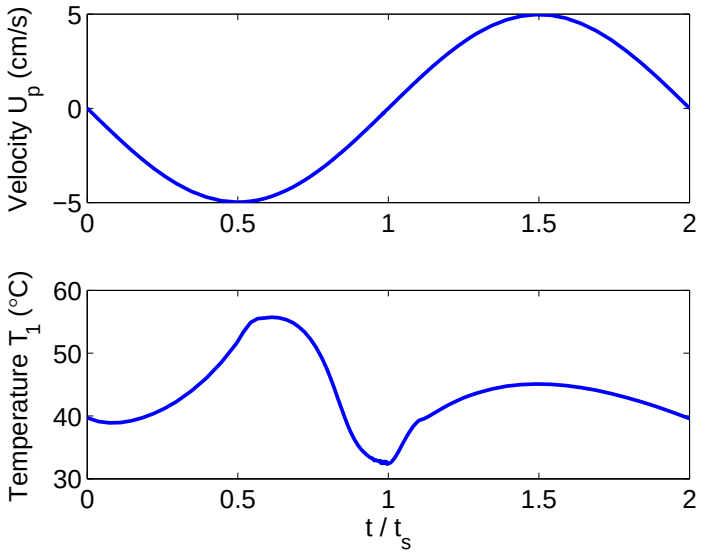

Figure A.4: Temperature profile in the compression chamber

At the beginning of the intake stroke, the inlet valve stays closed and the pressure decreases due to fluid expansion till it becomes less than the inlet pressure. When the intake valve opens, a

cooled fluid enters the chamber and mixes with the hotter fluid inside the chamber. This mixing makes the fluid temperature decrease and return to the initial values.

A.2.3 Effect of piston velocity changes

The piston movement causes changes in the volume of the compression chamber, which affects the temperature and pressure of the refrigerant. Figure A.5 shows the pressure and temperature profiles at three different mid-stroke speeds 3 cm/s, 5 cm/s and 7 cm/s.

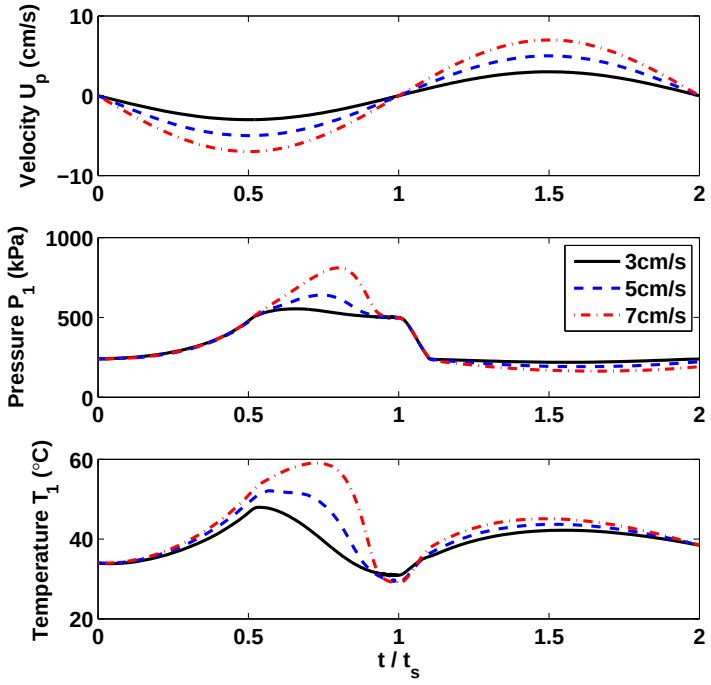

Figure A.5: Effect of piston velocity changes on pressure and temperature profiles in the compression chamber CV1

When the piston moves faster, the time required to finish the stroke becomes shorter. Consequently the power applied to the piston is higher. The higher force applied to the piston pushes the pressure and temperature of the compression chamber up to a higher value.

On the other hand, when the velocity of the piston becomes higher the differential pressure across the outlet valve becomes higher and the outlet flow rate increases. Figure A.6 shows the effect of changing the piston velocity on the mass flow rates across the valves. During the suction stroke the intake valve opens while the discharge valve remains closed. Moreover the discharge valve opens during the compression stroke only when the pressure inside the compres-

sion chamber becomes higher than the outlet pressure. Because of this behavior, the discharge flow oscillates and theoretically becomes zero during the suction stroke and at the beginning of the discharge stroke. In real compressors, inlet and exit manifolds exist as dampers to attenuate refrigerant flow oscillations.

The piston velocity has the same effect on the leakage flow rate through the leakage gap. As illustrated in Figure A.6, the main forces affecting the leakage flow rate are the pressure difference and piston movement.

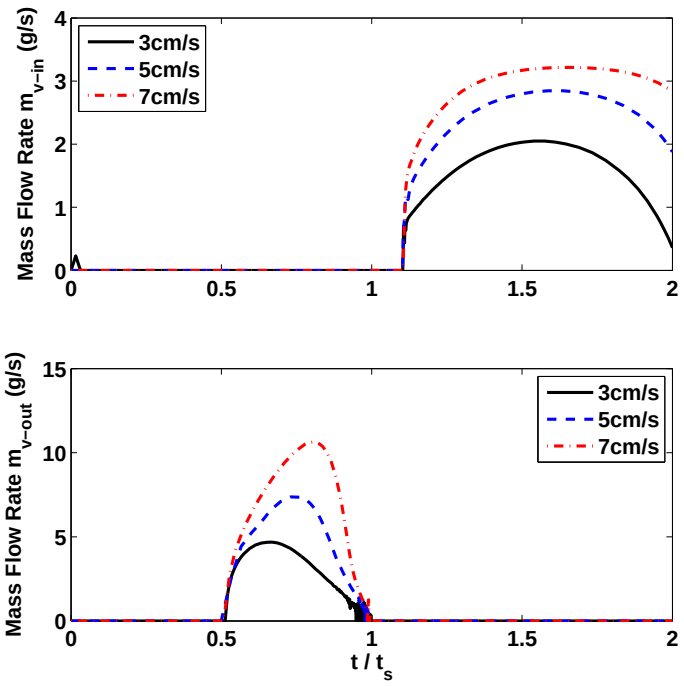

Figure A.6: Effect of piston velocity changes on mass flow rate across intake and discharge valves

Figure A.7 shows the effect of the piston velocity change on the leakage flow rate between the compression chamber and the second chamber CV2

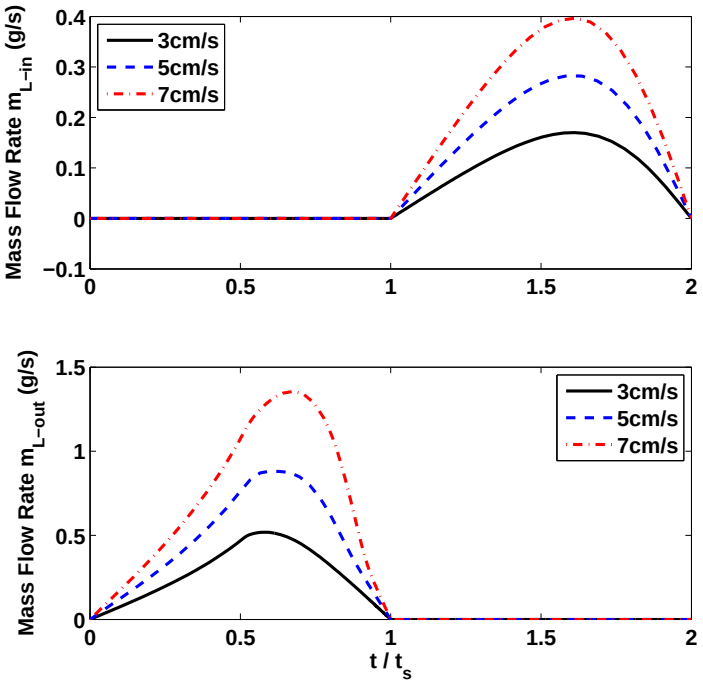

Figure A.7: Effect of piston velocity changes on leakage flow rate

A.2.4 Effect of piston displacement changes

In linear micro-compressors, compression flow rate, pressure and temperature are affected by the piston displacement changes. Reducing stroke length of the piston will affect the stroke time, as characterized by Eq.A.19. Figure A.8 shows the effect of reducing the stroke length on the pressure and temperature profiles inside the compression chamber.

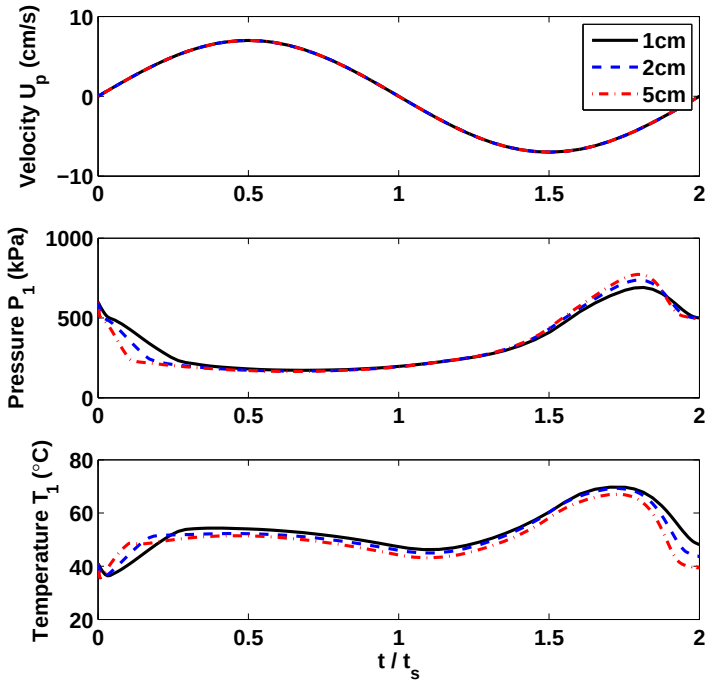

Figure A.8: Effect of piston displacement changes on pressure and temperature profiles in the compression chamber CV1

When the stroke length is reduced, the pressure inside the compression chamber takes more time to become lower than the inlet pressure. The intake valve will in turn be open for a shorter length of time. This will reduce the mass flow rate across the intake valve. In the compression stroke, reducing the stroke length will decrease the peak value of the pressure in the cycle. This will make the pressure difference across the discharge valve lower which will in turn affect the discharge flow rate, as described by Eq. A.21. Figure A.9 shows the influence of reducing the stroke length on the mass flow rates across the intake and discharge valves.

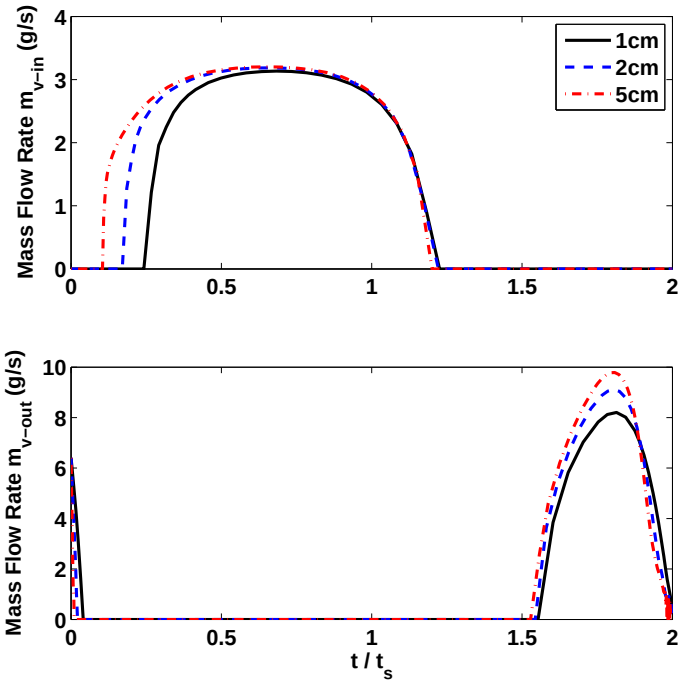

Figure A.9: Effect of piston displacement changes on mass flow rates across intake and discharge valves

A.2.5 Effect of piston motion profile on the pressure profile

The piston motion profile is assumed to be the same as the velocity profile for the crank-driven piston, which is a sine wave profile. It is clear from Figure A.3 that the pressure needs almost 50% of the compression stroke to reach the outlet pressure value. Also, in the suction stroke, the pressure barely becomes lower than the input pressure to allow the gas to flow into the compression chamber. This trend of pressure change affects the amount of the inlet and outlet flow rate as per Figure A.6. In order to enhance the compressor performance, the piston should reach the maximum velocity more quickly. Chen et al [19] proposed a profile which is very close to a square wave profile. The rapid change in the piston motion direction as well as the short time period for reaching the maximum velocity allows the pressure inside the compression chamber to increase much faster than the proposed profile in this study.

Appendix B

Nomenclature

A	Area $[m^2]$
A_l	Channel Flow Cross Sectional Area $[m^2]$
CAS	Chemical Abstracts Service
A_V	Valve Opening Position $[\%]$
b	Mean Channel Flow Gab $[m]$
CFC	Chlorofluorocarbon
CHF	Critical Heat Flux
COP	Coefficient of Performance
C_P	Heat Capacity $[J/(kg.K)]$
C_V	Flow Coefficient [-]
$CV1$	Control Volume 1
$CV2$	Control Volume 2
DAQ	Data Acquisition Unit
D_h	Hydraulic Diameter $[m]$
d	Diameter $[m]$
E	Total Energy $[J]$

f	Friction Factor [-]
G	Mass Flux $[kg/(m^2.s)]$
GWP	Glopbal Warming Potential
HC	Hydrocarbon
$HCFC$	Hydrochlorofluorocarbon
HFC	Hydrofluorocarbons
$HMIS$	Hazardous Materials Identification System
h	Enthalpy $[J/kg]$
k	Thermal Conductivity $[W/(m.K)]$
L	Length $[m]$
L_P	Plate Length $[m]$
L_w	Plate Width $[m]$
M	Molar Mass $[kg/kmol]$
$\dot{m}$	Mass Flow Rate $[kg/s]$
Nu	Nusselt Number [-]
ODP	Ozone-Depletion Potential
P	Pressure $[Pa]$
PHE	Plate Heat Exchanger
Pr	Prandtl Number [-]
$PTFE$	Polytetrafluoroethylene
p_w	Wetted Perimeter $[m]$
$\dot{Q}$	Heat Transfer $[W]$
Re	Reynolds Number [-]

T	Temperature $[K]$
TCB	Temperature Control Bath
TEC	Thermal Expansion Valve
t	Time $[s]$
t_s	Stroke Time $[s]$
u	Specific Internal Energy $[J/kg]$
U_p	Piston Velocity $[m/s]$
V	Volume $[m^3]$
VCC	Vapor Compression Cycle
$\dot{W}$	Work $[W]$
x	Quality [-]

Greek Letter

α	Heat Transfer Coefficient $[W/(m^2.K)]$
γ	Specific Heat Ratio [-]
δ	Radius Ratio [-]
η_s	Isentropic Efficiency [%]
η_v	Volumetric Efficiency [%]
μ	Dynamic Viscosity $[Pa.s]$
ρ	Density $[kg/m^3]$
ϕ	Effective Plate Length $[m/m]$

Subscripts

amb	Ambient
c	Condenser

cond	Condenser
Cr	Critical
crit	Critical
eq	Equivalent
e	Evaporator
evap	Evaporator
f	Saturated Liquid
g	Saturated Vapor
HX	Heat Exchanger
i	Inlet
l	Liquid
leak	leakage
lo	Liquid Only
m	mean
NBP	Normal Boiling Point
nc	Natural Convection
o	Outlet
p	Pipe
T	Total
sat	Saturation
sh	Shell
TP	Two Phase
v	Vapor

Vap	Vapor
w	Wall

Bibliography

[1] Air conditioning, 2013 (accessed May 15, 2014). URL http://www.powerwise.gov.ae/en/section/how-can-i-save-electricity/residential/air-conditioning.

[2] N. Acharya, M. Sen, and H.C. Chang. Analysis of heat transfer enhancement in coiled-tube heat exchangers. *International Journal of Heat and Mass Transfer*, 44(17):3189–3199, 2001.

[3] J. U. Ahamed, R. Saidur, and H. H. Masjuki. Prospect of hydrocarbon uses based on exergy analysis in the vapor compression refrigeration system. *IEEE First Conference on Clean Energy and Technology CET*, pages 300–304, 2011.

[4] W. W. Akers, H. A. Dean, and O. Crosser. Condensation heat transfer within horizontal tubes. *Chemical Engineering Progress*, 54:89–90, 1958.

[5] A. A. Al-Rashed. Effect of evaporator temperature on vapor compression refrigeration system. *Alexandria Engineering Journal*, 50(4):283–290, 2011.

[6] M. Alzoubi, G. Li, and T. J. Zhang. First-principle dynamic modeling of a linear micro-compressor. *International Mechanical Engineering Congress and Exposition*, 6B:–, 2013.

[7] C. Aprea, M. Ascani, and F. de Rossi. A criterion for predicting the possible advantage of adopting a suction/liquid heat exchanger in refrigerating system. *Applied Thermal Engineering*, 19(4):329–336, 1999.

[8] A. Arora and S. C. Kaushik. Theoretical analysis of a vapour compression refrigeration

system with R502, R404A and R507A. *International Journal of Refrigeration*, 31(6): 998–1005, 2008.

[9] R. C. Arora. *Mechanical Vapor Compression Refrigeration*. PHI Learning Private Limited, India, 2010.

[10] Z. Ayub. Status of enhanced heat transfer in systems with natural refrigerants. *Journal of Thermal Science and Engineering Applications*, 2(4):044001–044006, 2011.

[11] J. S. Baek, E. A. Groll, and P. B. Lawless. Piston-cylinder work producing expansion device in a transcritical carbon dioxide cycle. part II: theoretical model. *International Journal of Refrigeration*, 28(2):152–164, 2005.

[12] Chip Berry. End-use consumption of electricity, 2001 (accessed February 27, 2014). URL http://www.eia.gov/emeu/recs/recs2001/enduse2001/enduse2001.html.

[13] T. Bin, Z. Yuanyang, L. Liansheng, L. Guangbin, W. Le, and Y. Qichao. Thermal performance analysis of reciprocating compressor with stepless capacity control system. *Applied Thermal Engineering*, 54(2):380–386, 2013.

[14] C. R. Bradshaw, E. A. Groll, and S. V. Garimella. A comprehensive model of a miniature-scale linear compressor for electronics cooling. *International Journal of Refrigeration*, 34 (1):63–73, 2011.

[15] J. Catano, TJ. Zhang, J. T. Wen, M. K. Jensen, and Y. Peles. Vapor compression refrigeration cycle for electronics cooling part I: Dynamic modeling and experimental validation. *International Journal of Heat and Mass Transfer*, 66:911–921, 2013.

[16] C. Chang, N. Liang, and S. Chen. Miniature vapor compressor refrigeration system for electronic cooling. *IEEE Transactions on Components and Packaging Technologies*, 33 (4):794–800, 2010.

[17] Y. S. Chang, M. S. Kim, and S. T. Ro. Performance and heat transfer characteristics of hydrocarbon refrigerants in a heat pump system. *International Journal of Refrigeration*, 23(3):232–242, 2000.

[18] L. Chen, C. Wu, and F. Sun. Cooling load versus cop characteristics for an irreversible air refrigeration cycle. *Energy Conversion and Management*, 39(1–2):117–125, 1998.

[19] L. Chen, S. Xia, and F. Sun. Optimizing piston velocity profile for maximum work output from a generalized radiative law Diesel engine. *Mathematical and Computer Modelling*, 54(9-10):2051–2063, 2011.

[20] S. Cheng, S. Wang, and Z. Liu. Cycle performance of alternative refrigerants for domestic air-conditioning system based on a small finned tube heat exchanger. *Applied Thermal Engineering*, 64(1–2):83–92, 2014.

[21] S. W. Churchill and M. Bernstein. A correlating equation for forced convection from gases and liquids to a circular cylinder in crossflow. *Journal of Heat Transfer*, 99:300–306, 1977.

[22] S. W. Churchill and H. H. S. Chu. Correlating equations for laminar and turbulent free convection from a vertical plate. *International Journal of Heat and Mass Transfer*, 18(11): 1323–1329, 1975.

[23] D. Colbourne and K. O. Suen. Appraising the flammability hazards of hydrocarbon refrigerants using quantitative risk assessment model part I: modelling approach. *International Journal of Refrigeration*, 27(7):774–783, 2004.

[24] D. Colbourne and K. O. Suen. Appraising the flammability hazards of hydrocarbon refrigerants using quantitative risk assessment model part I: Model evaluation and analysis. *International Journal of Refrigeration*, 27(7):7844–793, 2004.

[25] J. M. Corbern, J. Segurado, D.l Colbourne, and J. Gonzlvez. Review of standards for the use of hydrocarbon refrigerants in A/C, heat pump and refrigeration equipment. *International Journal of Refrigeration*, 31(4):748–756, 2008.

[26] V. Gnielinski. New equations for heat and mass transfer in turbulent pipe and channel flow. *International Chemical Engineering*, 16(2):359–368, 1976.

[27] E. Granryd. Hydrocarbons as refrigerants an overview. *International Journal of Refrigeration*, 24(1):15–24, 2001.

[28] M. A. Hammad and M. A. Alsaad. The use of hydrocarbon mixtures as refrigerants in domestic refrigerators. *Applied Thermal Engineering*, 19(11):1181–1189, 1999.

[29] J. B. Jensen and S. Skogestad. Optimal operation of simple refrigeration cycles part I: Degrees of freedom and optimality of sub-cooling. *Computers and Chemical Engineering*, 31(5–6):712–721, 2007.

[30] H. Kim, C. Roh, J. Kim, J. Shin, Y. Hwang, and J. Lee. An experimental and numerical study on dynamic characteristic of linear compressor in refrigeration system. *International Journal of Refrigeration*, 32(7):1536–1543, 2009.

[31] I. K. Kim, J. H. Park, Y. H. Kwon, and Y. S. Kim. Experimental study on R-410a evaporation heat transfer characteristics in oblong shell and plate heat exchanger. *Heat Transfer Engineering*, 28(7):633–639, 2007.

[32] J. Kim and E. A. Groll. Feasibility study of a bowtie compressor with novel capacity modulation. *International Journal of Refrigeration*, 30(8):1427–1438, 2007.

[33] J. K. Kim and J. H. Jeong. Performance characteristics of a capacity-modulated linear compressor for home refrigerators. *International Journal of Refrigeration*, 36(3):776–785, 2012.

[34] S. A. Klein, D.T. Reindl, and K. Brownell. Refrigeration system performance using liquid-suction heat exchangers. *International Journal of Refrigeration*, 23:588–596, 2000.

[35] P. K. Kundu and I. M. Cohen. *Fluid Mechanics*. Academic Press, USA, 2008.

[36] G. Lampugnani and M. Zgliczynski. R290 as a substitute of R502 and R22 in commercial refrigeration and air conditioning. *International Compressor Engineering Conference*, pages 83–88, 1996.

[37] H. Lee, J. Yoon, J. Kim, and P. K. Bansal. Condensing heat transfer and pressure drop characteristics of hydrocarbon refrigerants. *International Journal of Heat and Mass Transfer*, 49(11–12):1922–1927, 2006.

[38] K. Liang, R. Stone, M. Dadd, and P. Bailey. A novel linear Electromagnetic-Drive Oil-Free Refrigeration Compressor using R134a. *International Journal of Refrigeration*, 40 (0):450–459, 2014.

[39] S. Mancin, C. Zilio, G. Righetti, and L. Rossetto. Mini vapor cycle system for high density electronic cooling applications. *International Journal of Refrigeration*, 36(4):1191–1202, 2013.

[40] R. Mastrullo, A. W. Mauro, S. Tino, and G. P. Vanoli. A chart for predicting the possible advantage of adopting a suction/liquid heat exchanger in refrigerating system. *Applied Thermal Engineerin*, 27(14–15):2443–2448, 2007.

[41] A. F. Mills. *Heat Transfer*. Prentice Hall, USA, 1999.

[42] M. Mohanraj, S. Jayaraj, and C. Muraleedharan. Environment friendly alternatives to halogenated refrigerantsa review. *International Journal of Greenhouse Gas Control*, 3(1): 108–119, 2009.

[43] M. J. Moran and H. N. Shapiro. *Fundamentals of Engineering Thermodynamics*. John Wiley & Sons, USA, 2008.

[44] P. Naphon and S. Wongwises. A review of flow and heat transfer characteristics in curved tubes. *Renewable and Sustainable Energy Reviews*, 10(5):463–490, 2006.

[45] E. Navarro, I. O. Martinez-Galvan, J. Nohales, and J. Gonzalvez-Macia. Comparative experimental study of an open piston compressor working with R-1234yf, R-134a and R-290. *International Journal of Refrigeration*, 36(3):768–775, 2013.

[46] A. G. A. Nnanna. Application of refrigeration system in electronics cooling. *Applied Thermal Engineering*, 26(1):18–27, 2006.

[47] B. Palm. Hydrocarbons as refrigerants in small heat pump and refrigeration systems A review. *International Journal of Refrigeration*, 31(4):552–563, 2008.

[48] C. D. Perez-Segarra, J. Rigola, M. Soria, and A. Oliva. Detailed thermodynamic characterization of hermetic reciprocating compressors. *International Journal of Refrigeration*, 28(4):579–593, 2005.

[49] B.S. Petukhov. Heat transfer and friction in turbulent pipe flow with variable physical properties. *Advances in heat transfer*, 6:503–564, 1970.

[50] R. L. Pradhan, D. Ravikumar, and D. L. Pradhan. Review of nusselt number correlation for single phase fluid flow through a plate heat exchanger to develop c code application software. *Journal of Mechanical and Civil Engineering*, 4:1–8, 2013.

[51] G. B. Ribeiro. Development and analysis of a compact cooling system using the micro-compressor. *13th IEEE ITHERM Conference*, pages 717–722, 2012.

[52] J. Rigola, C. D. Perez-Segarra, and A. Oliva. Parametric studies on hermetic reciprocating compressors. *International Journal of Refrigeration*, 28(2):253–266, 2005.

[53] M. M. Shah. A general correlation for heat transfer during film condensation inside pipes. *International Journal of Heat and Mass Transfer*, 22(4):547–556, 1979.

[54] P. Thomas. *Simulation of Industrial Processes for Control Engineers*. Butterworth-Heinemann, USA, 1999.

[55] E. Torrella, J. A. Larumbe, R. Cabello, R. Llopis, and D. Sanchez. A general methodology for energy comparison of intermediate configurations in two-stage vapour compression refrigeration systems. *Energy*, 36(7):4119–4124, 2011.

[56] S. Trutassanawin, E. A. Groll, S. V. Garimella, and L. Cremaschi. Experimental investigation of a miniature-scale refrigeration system for electronics cooling. *IEEE Transactions on Components and Packaging Technologies*, 29(3):678–687, 2006.

[57] J. H. Wu, L. D. Yang, and J. Hou. Experimental performance study of a small wall room air conditioner retrofitted with R290 and R1270. *International Journal of Refrigeration*, 35(7):1860–1868, 2012.

[58] Z. Wu and R. Du. Design and experimental study of a miniature vapor compression refrigeration system for electronics cooling. *Applied Thermal Engineering*, 31(2–3):385–390, 2011.